



Parameterization model of soil thermal conductivity and its application in the permafrost region of the Qinghai-Tibet Plateau

Yizhen Du¹ · Jie Ni¹ · Ren Li² · Tonghua Wu^{2,3} · Guojie Hu² · Shuhua Yang⁴ · Xuefei Weng¹

Received: 14 December 2023 / Accepted: 7 February 2024 / Published online: 23 February 2024
© The Author(s), under exclusive licence to Springer-Verlag GmbH Austria, part of Springer Nature 2024

Abstract

Soil thermal conductivity (STC), which describes the ability of soil to transfer heat, is critical to understanding the thermal regime. Simulations of the heat of the permafrost regions on the Qinghai-Tibet Plateau (QTP) are currently inaccurate. This is partly because the current STC models used in the land surface models are not adequate to accurately reflect the characteristics of the ice-water phase change. Here, the new STC model was developed by dividing three different stages. Our analyses revealed that the soil moisture (θ_w) undergoes a rapid phase change in the $-2.5 \sim 0$ °C, where minor temperature changes could cause larger θ_w changes. When the temperature is below -2.5 °C, the θ_w mostly remains stable. Considering the influence of various factors in different temperature ranges, an improved STC model was proposed by piecewise fitting at 0 °C and -2.5 °C for the depths of 10–50 cm. Independent test results showed that the new model significantly improved simulation accuracy of STC in permafrost regions and was better able to reflect its changing characteristics, especially in the 50 cm depth. Lastly, the daily STC product in the permafrost region of the QTP was estimated with the new model. The average STC during 1982 to 2020 was about $0.495 \text{ Wm}^{-1}\text{K}^{-1}$, showing a spatial pattern of low in the northwest and high in the southeast. In addition, the STC showed a tiny increasing trend at a rate of $0.008 \text{ Wm}^{-1}\text{K}^{-1}/10\text{a}$. Spatially, the regions with the highest rates of increase were concentrated in the eastern, southeastern, and south-western regions, which comprise mostly unstable and extremely unstable permafrost. This study deepened our understanding of the STC during the freeze–thaw cycle and provides data products for further studies on the soil thermal state in permafrost regions.

1 Introduction

Known as the “Third Pole of the Earth,” the Qinghai-Tibet Plateau (QTP) plays an essential role in Asian monsoon system and climate change (Ma et al. 2011; Tang et al. 1979). It has the highest elevation, widest area, and thickest permafrost

in the mid- and low-latitude regions, accounting for approximately 42.4% ($1.06 \times 10^6 \text{ km}^2$) of the QTP (Zhao et al. 2017; Zou et al. 2017). Permafrost refers to soil, rocks, or sediments that have a temperature at or below 0 °C for at least two consecutive years and is a key component of the cryosphere (Riseborough et al. 2008). Compared with the high-latitude regions, the permafrost on the QTP is more sensitive to climate change due to their relative thin thickness, high ground temperature, uneven distribution, and poor stability (Qin et al. 2020; Xu and Wu 2019). These characteristics exacerbate the degradation of the permafrost, which is manifested as a rise in soil temperature, a thickening of the active layer, and the occurrence of freeze–thaw disasters such as thermal thaw subsidence and slump (Hjort et al. 2022; Ni et al. 2020; 2022). In recent years, considerable efforts have gone into investigating the changes of the permafrost and predicting its future. One of the important aspects is the study of soil thermal conductivity (STC) in permafrost. STC, which characterizes the heat transfer capacity of the soil, affects water and energy exchange between surface and deep soil (Cui et al. 2020; De Vries 1963). Under the global warming, STC can affect the

Yizhen Du and Jie Ni contributed equally to this article.

✉ Ren Li
liren@lzb.ac.cn

- ¹ College of Tourism, Resources and Environment, Zaozhuang University, Zaozhuang, China
- ² Cryosphere Research Station On the Qinghai-Tibet Plateau, State Key Laboratory of Cryospheric Sciences, Northwest Institute of Eco-Environment and Resources, Chinese Academy of Sciences, 320 Donggang West Road, Lanzhou 730000, China
- ³ Southern Marine Science and Engineering Guangdong Laboratory, Guangzhou 511458, China
- ⁴ School of Environmental Sciences, Nanjing Xiaozhuang University, Nanjing 211171, China

response of permafrost to external thermal disturbance and plays an important role in the study of soil freeze–thaw depth and engineering stability, such as the embankments, the tunnels, and the pipelines (Chen et al. 2021; Mu et al. 2020; Pei et al. 2019; 2022). Moreover, as a key input parameter of land surface models, accurate STC value significantly affects the simulation results of soil temperature and surface energy balance (Dai et al. 2019; Li et al. 2019; Yang et al. 2021). However, the research in this area is still insufficient and needs to be further explored.

Direct observation and model calculation can both estimate the STC. At present, direct observations can obtain accurate values on the point scale by steady-state or transient methods (Tao and Zhang 1983; Yu et al. 2014). However, direct observations are generally time-consuming and labor-intensive and also can be easily affected by the observing environment. Especially in extreme-cold areas such as the QTP, the lack of oxygen combined with the harsh nature of the environment makes it difficult to achieve detailed field observations on large scales. So, it is difficult to systematically conduct a series of studies on hydrothermal dynamics because of the limited observational data (Li et al. 2019). Therefore, a simple and accurate calculation model of STC based on field observations is necessary to understand the changes in soil moisture (θ_w) and heat transport in the permafrost regions of the QTP. Recently, considerable efforts have been devoted to characterizing the relationship between various factors and STC and then developing STC models under distinct conditions.

De Vries (1963) regarded soil as a mixture of ellipsoidal particles in a continuum and established a theoretical STC model under unsaturated and unfrozen conditions. This model has been widely used in STC modeling with superior accuracy. However, it is mostly suitable for unfrozen soil with a saturation level of 10–20% (Nikolaev et al. 2013) due to the selection of critical θ_w and form factor in the model calculation (Ochsner et al. 2001). Tian et al. (2016) adjusted the parameters in the De Vries model and redefined the “continuum,” which improved the simulated accuracy (He et al. 2021a). But the Tian model would underestimate STC under conditions of low θ_w (Yan et al. 2019). Furthermore, more empirical and semi-empirical models have also been developed. Based on the results of over 1000 tests on 19 different soil types, Kersten (1949) established an empirical formula for STC that was simple to calculate but generally not suitable for use at low θ_w (Zhao et al. 2019a). Based on the Kersten model and a large number of experimental studies, Johansen (1975) proposed the concept of normalized STC (K_e) and established a STC model based on the relationship between K_e and saturation. In subsequent studies, the Johansen model has been widely applied and evaluated for different conditions and, in general, is superior to other schemes, especially in permafrost regions (Dai et al. 2019; Peters-Lidard et al. 1998). However, the Johansen

model is sensitive to quartz content, soil porosity, and other soil parameters (Balland and Arp 2005; He et al. 2019). Therefore, improvements have been made to improve the accuracy of STC calculations under different ranges of soil parameters (Balland and Arp 2005; Côté and Konrad 2005; Farouki 1981; Lu et al. 2007; Zhao et al. 2019a; Zhao and Si 2019). In addition to the development of these STC models, machine learning methods have also been used to calculate STC, such as artificial neural network, K -nearest neighbors, extreme learning machine, multilayer perceptron, support vector machine, and decision tree, which provide new light on STC (Dong et al. 2022; Li et al. 2023; Sargam et al. 2021; Wang et al. 2023; Zhang et al. 2020a; 2020b).

Although the accuracy of the improved models has been enhanced to a certain extent compared with the original, most of them still cannot give accurate STC values for permafrost (He et al. 2021a). This is mainly because the dynamic mechanisms of change for STC are highly complicated under the influence of θ_w , solid ice content, soil temperature, mineral composition, particle size composition, porosity, and many other factors (He et al. 2017; 2021b; Malek et al. 2021; Nikoosokhan et al. 2016). Among them, θ_w plays a crucial role (Farouki 1981; Johansen 1975; Yan et al. 2019). Moreover, the presence and content of solid ice in the soil can affect the mobility of soil liquid water and drastically change the thermal properties of the soil during the frozen period. This is because there is a large difference between the thermal conductivity of ice ($2.29 \text{ Wm}^{-1}\text{K}^{-1}$) and that of water ($0.57 \text{ Wm}^{-1}\text{K}^{-1}$). In the negative temperature range near 0°C , liquid water has a drastic phase transition zone, which can significantly change the thermal properties of frozen soil (Bao et al. 2016; Hu et al. 2020a; Ochsner and Baker 2008; Tian et al. 2020; Zhao et al. 2019b). Consequently, it is necessary to study the STC at different negative temperatures.

By comparing the applicability of several calculation models in permafrost regions, Du et al. (2020) selected the STC models with the best performance in frozen and thawed periods, respectively. However, when we concatenated the results of Du et al. (2020) during the frozen and thawed periods, errors in the calculations near 0°C still existed (Fig. 1), which is consistent with the results of previous studies as well (He et al. 2021a; Kojima et al. 2016). That is, due to the large difference between the thermal conductivity of ice and water, the STC can be significantly affected by the extent of the ice–water phase change with temperature at different stages of the freeze–thaw cycle. However, the current STC models were mainly calculated by 0°C division. This division leads to the neglect of the drastic fluctuation of STC caused by the rapid ice–water phase transition (Li et al. 2019), which affects the accuracy of the STC simulation. Hence, it is necessary to propose a more reasonable model to evaluate the STC characteristics of the permafrost on the QTP.

This research aimed to (a) divide a temperature range where liquid water changes from rapid phase transitions to stable

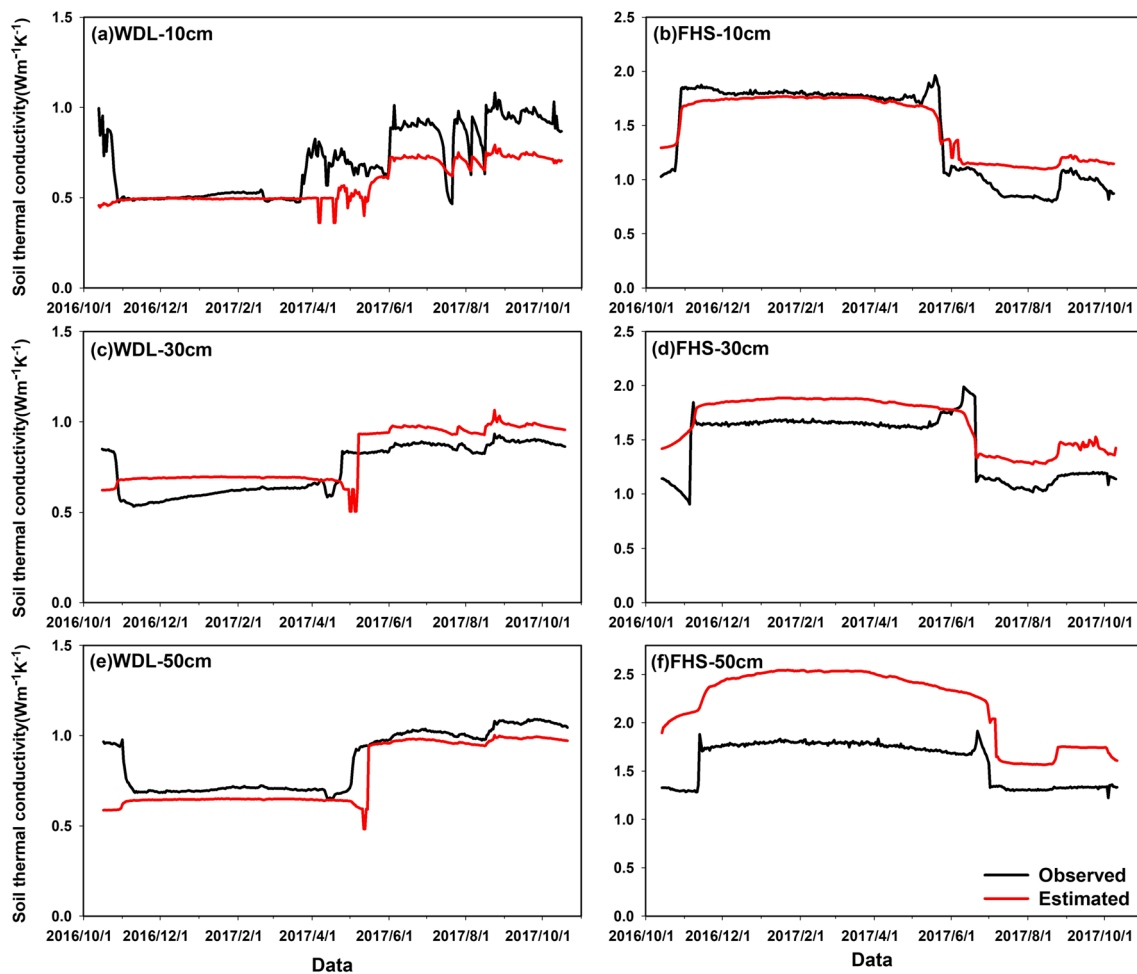


Fig. 1 Comparison between soil thermal conductivity values of observed and estimated by the best schemes based on Du et al. (2020) at WDL and FHS sites

changes, (b) develop a new model under different temperature ranges, (c) produce the dataset of STC in the permafrost regions of the entire QTP, and (d) analyze the temporal and spatial characteristics of STC for the permafrost regions. It is meant to provide basic input parameter for land surface model, thus, ultimately contributing to a better understanding of the degradation of frozen soils.

2 Data and methods

2.1 Data

2.1.1 Observational sites and data

In this study, six observational sites were chosen in the permafrost area of the central QTP: Xidatan (XDT), Kunlunshan (KLS), Tedaqiao (TDQ), Qingshuihe (QSH), Wudaoliang (WDL), and Fenghuoshan (FHS) (Fig. 2). The

study area covered the main types of underlying surface, such as alpine meadow, alpine swamp meadow, alpine steppe, alpine desert, and alpine desert steppe in the permafrost region of the QTP. With an average elevation of more than 4500 m, the study area belongs to the sub-frigid and semi-arid climate zones (Lin and Wu 1981), which are generally representative of the QTP. The average annual near-surface (2 m) temperature is about -5.5 to -3.1 °C. Besides, the annual average relative humidity ranges from 55.2 to 53.3%, and precipitation is mainly concentrated from May to September. The characteristics of the observational sites are listed in Table 1.

At each observational site, five soil parameters were collected, including STC, soil temperature, θ_w , dry bulk density of the soil (ρ_d), and particle size.

1. The first three data parameters were collected by the Cryosphere Research Station on the QTP, Chinese Academy of Sciences, from October 1, 2016, to September

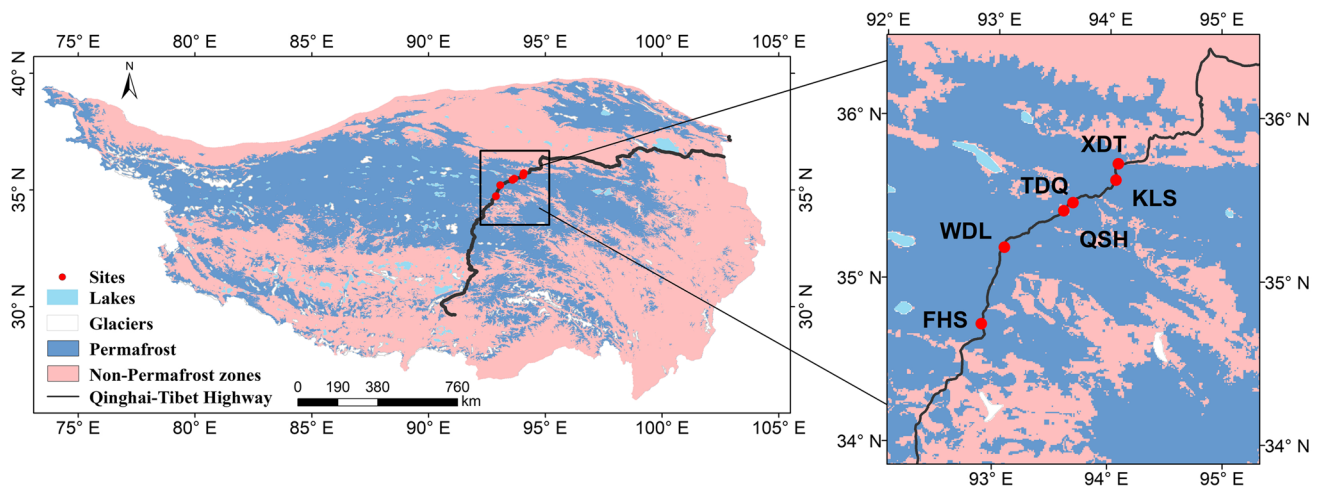


Fig. 2 The spatial distribution of the observational sites used in the study. The distribution maps of the permafrost and non-permafrost zone were derived from Zou et al. (2017)

30, 2017. The STC measurements were determined by a TP01 instrument with an accuracy of $\pm 0.05 \text{ Wm}^{-1}\text{K}^{-1}$. Soil temperature was measured using 105T Thermocouple Probe with a precision of $\pm 0.1 \text{ }^\circ\text{C}$. The θ_w was measured using a Hydra soil moisture sensor with an accuracy of $\pm 3\%$. All data were recorded every 30 min using a CR1000 datalogger (Li et al. 2019; Zhao et al. 2021). In this study, owing to a large number of invalid θ_w at deep layers, the research was carried out at depths of 10–50 cm.

2. The remaining two parameters were obtained through laboratory experiments. Soil samples were collected vertically along the test pit profiles by employing cutting rings at different depths. Then, the soil samples were weighed, oven-dried at $105 \text{ }^\circ\text{C}$ for 24 h in the laboratory, and weighed again to calculate the ρ_d . The dry soil samples were then ground and sieved (Duan et al. 2021, 2022; Yan et al. 2021). Soil particle sizes were determined using a Malvern Mastersizer 2000 particle size analyzer (<http://www.malvern.com>). Lastly, the soil textures at different depths at observational sites were classified based on the classification provided by the United States Department of Agriculture (USDA).

Before the development of the new model, the soil at different depths in a given observation site had been randomly divided into a training portion and a testing portion, ensuring that both portions contained soil samples within a depth of 10–50 cm. Thus, the 10 cm depth of QSH, 20 cm depth of KLS, and 50 cm depth of FHS were randomly selected and classified as the testing portion which was utilized to evaluate the accuracy of the new model. The remaining depths were used for training portion which was applied to develop the new model.

2.1.2 ERA5 reanalysis product

The European Centre for Medium-Range Weather Forecasts (ECMWF) Reanalysis v5 (ERA5) global reanalysis product, an alternative to the ERA-Interim, is the fifth generation of meteorological reanalysis dataset published by the ECMWF and covers historical data from 1981 to the present. Compared to the ERA-Interim product (Dee et al. 2011), ERA5 significantly improves data accuracy by using several integrated forecasting systems (Czernecki et al. 2019; Hersbach et al. 2019). Additionally, the ERA5 data has higher

Table 1 Information for the observational sites used in the study (Yue et al. 2017)

Site	Longitude ($^\circ\text{E}$)	Latitude ($^\circ\text{N}$)	Elevation (m)	Land surface type	Coverage (%)
Xidatan (XDT)	94.08	35.72	4516	Alpine meadow	85.0
Kunlunshan (KLS)	94.06	35.62	4747	Alpine desert	12.3
Tedaqiao (TDQ)	93.68	35.49	4529	Alpine steppe	23.3
Qingshuihe (QSH)	93.60	35.43	4468	Alpine meadow	60.2
Wudaoliang (WDL)	93.08	35.20	4637	Alpine desert steppe	11.7
Fenghuoshan (FHS)	92.89	34.73	4772	Alpine swamp meadow	69.3

spatial–temporal resolution and more product parameters. It is found that the soil temperature and water data from ERA5 have better performance in the QTP (Cheng et al. 2019; Yang et al. 2020; Zhao et al. 2019c). To meet the requirements of the QTP simulations, we made the following adjustments to the data:

1. Since the data collection of ERA5 products adopts universal time, we adjusted the time to Beijing time, i.e., universal time + 8 h.
2. The data of the first two-layer depths of the dataset (i.e., 0–7 cm and 7–28 cm) were weighted and averaged to obtain the data of 0–28 cm depth;
3. The humidity data from ERA5 refers to the total soil water content, i.e., the θ_w in the thawed period, and the sum of the θ_w and the solid ice content in the frozen period. Additionally, this study required a value for the θ_w . Hu et al. (2020b) evaluated the applicability of various formulas for calculating the θ_w under the negative temperature and found that the scheme of Zhang et al. (2017a) performed relatively well. Therefore, we used Zhang et al. (2017a) to calculate the θ_w from the ERA5 data as follows:

$$\theta_w = \bar{\theta} \left(1 - \left(\frac{T_f - T}{273.15 + T_f} \right)^\beta \right), T < T_f \tag{1}$$

where $\bar{\theta}$ is the mean θ_w when the temperature is greater than 0 °C; T_f is the freezing point, which is regarded as 0 °C in the study; T refer to the soil temperature; β is the fitting parameter; and the suggested value is 0.94 based on the fitting result of the hydrothermal observation data of the active layer (Hu et al. 2020b).

2.1.3 Soil dataset of QTP

The soil dataset used in this study to simulate the STC in the permafrost regions of the entire QTP was from the Genetic Soil Data Environment (GSDE; a Chinese dataset of soil properties for land surface modeling, <http://westdc.westgis.ac.cn/data>) developed by Shangguan et al. (2013). The GSDE offers basic soil property information such as particle-size distributions, organic carbon, and nutrients at a resolution of 0.00833° with a depth of 0–3 m using a linkage method based on the world soil map by Shi et al. (2004). Shangguan et al. (2013) used the Harmonized World Soil Database (HWSD) to evaluate the GSDE and found that the GSDE had higher spatial accuracy and more reasonable spatial magnitudes. For this study, we selected the soil texture and ρ_d from the GSDE. To meet the requirements of the simulation on the QTP, data from the first four depths of the GSDE, namely, 0–4.5 cm, 4.5–9.1 cm, 9.1–16.6 cm, and

16.6–28.9 cm, were weighted and averaged to obtain soil data at 0–28 cm depths. Moreover, to match the ERA5 reanalysis data, the resolution of GSDE was resampled to 0.1°.

2.2 Existing models for soil thermal conductivity

In this study, the development of the new model was based on the STC model by Johansen (1975). Using experimental data (Kersten 1949; Smith and Byers 1938; Smith 1942), Johansen (1975) first introduced the normalized thermal conductivity concept, K_e (i.e., the Kersten’s number) and proposed a model based on the relationship between the STC, K_e , and soil saturation level (S_r) for unsaturated soils:

$$\lambda = \begin{cases} (\lambda_{\text{sat}} - \lambda_{\text{dry}})K_e + \lambda_{\text{dry}} & S_r > 1 \times 10^{-5} \\ \lambda_{\text{dry}} & S_r \leq 1 \times 10^{-5} \end{cases} \tag{2}$$

$$K_e = \begin{cases} 0.7 \log S_r + 1.0 & 0.05 < S_r < 0.1, \text{ coarse soil, unfrozen} \\ \log S_r + 1.0, & 0.1 < S_r, \text{ fine soil, unfrozen} \\ S_r, & \text{frozen soil} \end{cases} \tag{3}$$

$$\lambda_{\text{dry}} = \frac{0.135 * \rho_d + 0.0647}{\rho_s - 0.947 * \rho_d} \tag{4}$$

$$\lambda_{\text{sat}} = \begin{cases} \lambda_s^{1-\theta_{\text{sat}}} \lambda_w^{\theta_{\text{sat}}}, & T \geq T_f \\ \lambda_s^{1-\theta_{\text{sat}}} \lambda_w^{\theta_w} \lambda_{\text{ice}}^{\theta_{\text{sat}}-\theta_w}, & T < T_f \end{cases} \tag{5}$$

where λ is the estimated STC ($\text{Wm}^{-1}\text{K}^{-1}$), and λ_{sat} and λ_{dry} are the saturated and dry STC ($\text{Wm}^{-1}\text{K}^{-1}$), respectively. ρ_d and ρ_s are the soil dry density (gcm^{-3}) and soil particle density, respectively. θ_{sat} is the soil saturated water content ($\text{m}^3 \text{m}^{-3}$). λ_w and λ_{ice} are the thermal conductivity of water ($0.57 \text{Wm}^{-1}\text{K}^{-1}$) and ice ($2.29 \text{Wm}^{-1}\text{K}^{-1}$), respectively. λ_s are the thermal conductivity of solid by $\lambda_s = \lambda_q^q \lambda_o^{1-q}$; λ_q is the thermal conductivity of quartz ($7.7 \text{Wm}^{-1}\text{K}^{-1}$); λ_o is the thermal conductivity of other minerals; it is suggested to be $2.0 \text{Wm}^{-1}\text{K}^{-1}$ for the quartz content (q) > 0.2 and $3.0 \text{Wm}^{-1}\text{K}^{-1}$ for $q \leq 0.2$ (Johansen 1975); q is assumed to be 50% of the sand content (Du et al. 2020; He et al. 2021a).

$$S_r = \theta_{\text{tot}}/n \tag{6}$$

where n is porosity, and θ_{tot} means the total water content, which implies the θ_w at the positive temperature and the sum of the θ_w and solid ice contents (θ_{ice}) at negative temperatures, respectively. For frozen soil, assume that once frozen, the liquid water in the soil no longer migrated, and θ_{ice} at a certain depth under frozen state (Tarnawski and Wagner 1993) was expressed as

$$\theta_{ice} = (\theta_{ini} - \theta_w) \frac{\rho_w}{\rho_{ice}} \quad (7)$$

where ρ_w and ρ_{ice} are the density of water and ice, respectively. θ_{ini} is the initial value during the frozen period ($\text{m}^3 \cdot \text{m}^{-3}$), which refers to θ_w at the depth on the date of freezing (Zhao et al. 2004).

Validation of the new model was obtained by comparing with the Johansen model, Campbell model (Campbell, 1985), C&K model (Côté and Konrad 2005), He model (He et al. 2017), and Bao model (Bao et al. 2016). The first four models performed better in the evaluation study by Du et al. (2020). The Bao model (Bao et al. 2016) was derived by incorporating the influence of λ_{ice} into the Johansen model and Yang model (Yang et al. 2005).

2.3 Evaluation metrics

Four evaluation indices were used to evaluate the performance of the model: (1) the root mean square error (RMSE), (2) the mean absolute error (MAE), (3) the mean bias error (MBE), and (4) the coefficient of determination (R^2). They were calculated as follows:

$$\text{RMSE} = \sqrt{\frac{\sum_{i=1}^N (E_i - O_i)^2}{N}} \quad (8)$$

$$\text{MAE} = \frac{\sum_{i=1}^N |E_i - O_i|}{N} \quad (9)$$

$$\text{MBE} = \frac{\sum_{i=1}^N (E_i - O_i)}{N} \quad (10)$$

$$R^2 = \left(\frac{\sum_{i=1}^N (E_i - \bar{E})(O_i - \bar{O})}{\sqrt{\sum_{i=1}^N (E_i - \bar{E})^2} \sqrt{\sum_{i=1}^N (O_i - \bar{O})^2}} \right)^2 \quad (11)$$

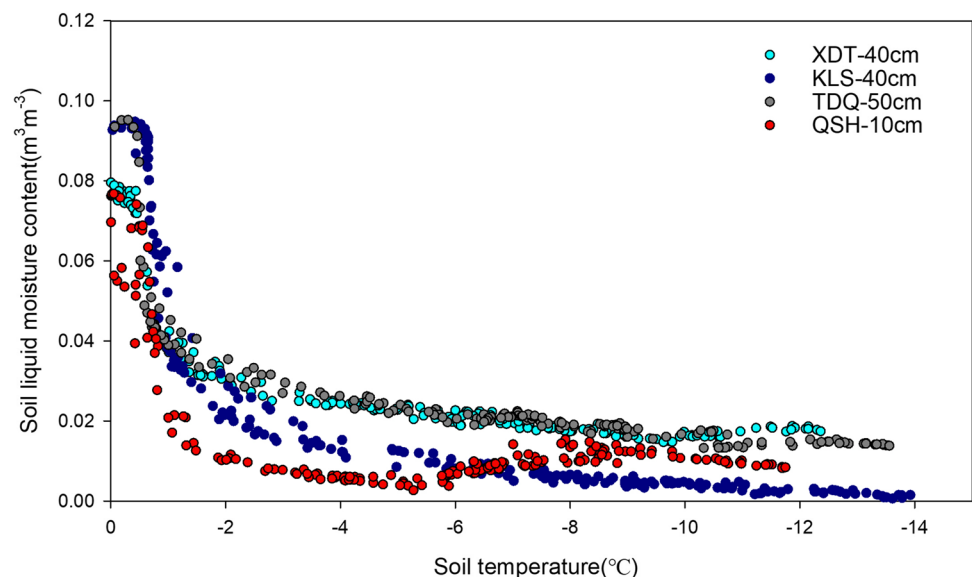
where E_i and O_i are the estimated and observed values, respectively; \bar{O}_i is the mean value of the observed data; and N means the number of observations in the dataset.

3 Results and discussion

3.1 Development of the new STC model

It is well-known that θ_w is an exponential function of soil temperature in the frozen state (Farouki 1981; Hu et al. 2023). In addition, soil temperature always affects the variability of θ_w and STC during the freeze–thaw cycle. At a negative temperature near 0 °C, there is a phase where the θ_w changes dramatically. As shown in Fig. 3, when the soil temperature begins to fall below 0 °C, a large amount of liquid water will rapidly condense into solid ice, and the θ_w will decrease rapidly. Even a slight change in the soil temperature during this period could induce a noticeable change in θ_w . After reaching a certain temperature node, the θ_w remains fundamentally constant, fluctuating only within a small range, even when the soil temperature changed dramatically. This variation of the θ_w with the soil temperature was essentially the same at different soils, but these temperature nodes varied. In this study, “the capture percentage” of the temperature node was defined as the percentage of the rapid changing period to the actual rapid changing period of the moisture content. We selected –1 °C, –1.5 °C, –2 °C, –2.5 °C, and –3 °C as temperature nodes and compared

Fig. 3 Variation in the soil liquid moisture under the negative soil temperature



their capture percentage. As shown in Table 2, the capture percentage of different temperature nodes traces a parabolic curve reaching a peak at $-2.5\text{ }^{\circ}\text{C}$. Hence, $-2.5\text{ }^{\circ}\text{C}$ was identified as the temperature node where θ_w changed from rapid to stable states at negative temperatures.

In the STC calculation models, K_e was mostly calculated as a function of S_r under positive temperature which was an improvement on the Johansen model and was assumed to be equal to S_r under negative temperature. In other words, the relationship between K_e and S_r was explored independently at positive and negative temperatures. In the study, we assumed $0\text{ }^{\circ}\text{C}$ and $-2.5\text{ }^{\circ}\text{C}$ as the temperature segments to analyze the relationships between K_e and S_r under different temperature ranges (Fig. 4). It should be noted that, as K_e is not an inherent

property of soil but a concept of normalized STC, the value of K_e cannot be obtained through actual measurement. In this study, the K_e value of soil samples was inversely derived under Eq. (2), Eq. (5), and $\text{Du}-\lambda_{\text{dry}}$ scheme (Du et al. 2022). It can be seen that when soil temperature $>0\text{ }^{\circ}\text{C}$, S_r increased with the occurrence of soil thawing and rainfall, and the soils consistently displayed a logarithmic increasing trend in K_e . When the soil temperature was less than $0\text{ }^{\circ}\text{C}$, the S_r was fundamentally unchanged, but the K_e value fluctuated within a certain range, especially in the $-2.5\sim 0\text{ }^{\circ}\text{C}$ temperature range, where the fluctuation reached up to 0.6. Hence, setting K_e equal to S_r under negative soil temperatures would lead to large calculation errors and eventually to an inaccurate STC during the frozen period, especially in the temperature range of $-2.5\sim 0\text{ }^{\circ}\text{C}$. We then performed a stepwise regression of the effect of soil properties on K_e in different temperature ranges (Table 3). When soil temperature $\geq 0\text{ }^{\circ}\text{C}$, the change in K_e is deeply affected by the θ_w and ρ_d , while, under negative temperatures, θ_{tot} and soil clay content determine K_e , but the influence degree of the above two factors is different in $0\sim -2.5\text{ }^{\circ}\text{C}$ range and less than $-2.5\text{ }^{\circ}\text{C}$, respectively. Then, the formula for K_e in different temperature ranges was established as follows:

Table 2 The capture percentage of the temperature node for rapid changing period

Temperature node ($^{\circ}\text{C}$)	Capture percentage (%)	Temperature node ($^{\circ}\text{C}$)	Capture percentage (%)
-1	49.0%	-2.5	64.8%
-1.5	58.6%	-3	63.3%
-2	63.5%		

Bold data represents the best result

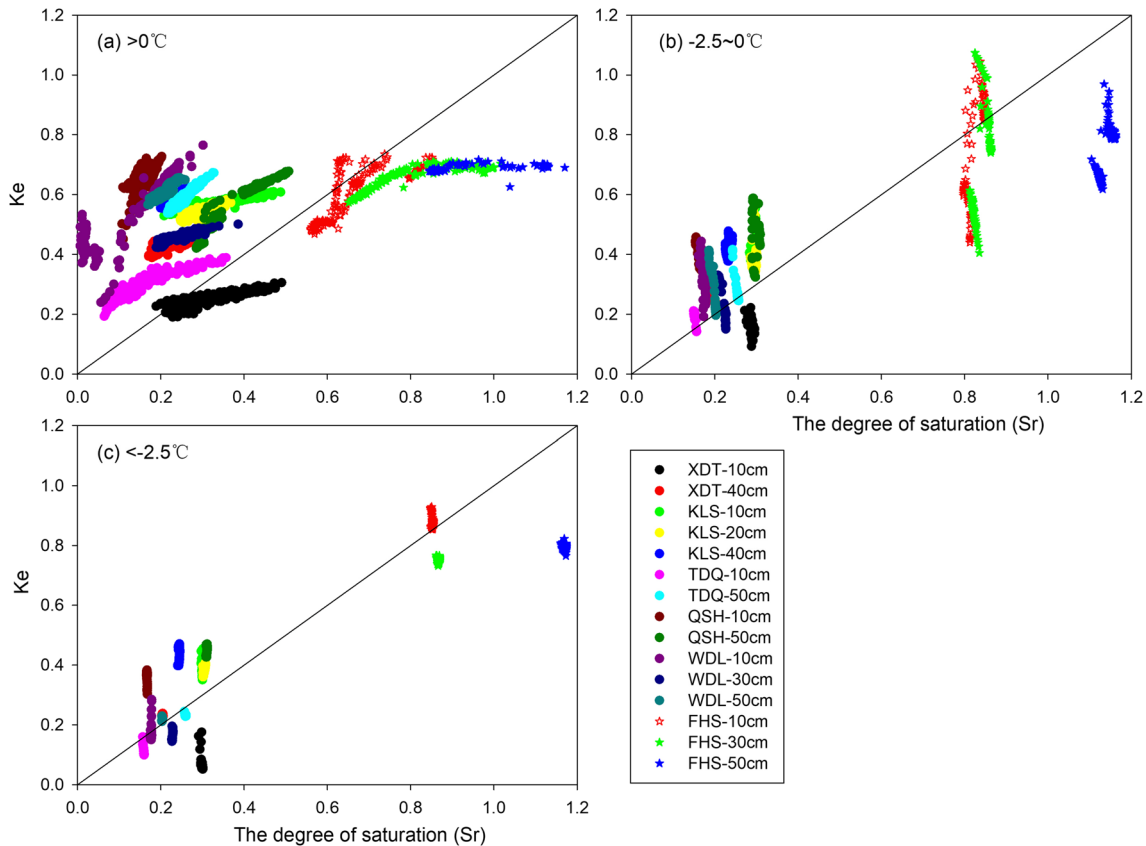


Fig. 4 The relationship between K_e and degree of saturation under different ranges of soil temperature

$$K_e = \begin{cases} 0.173 + 0.544 \exp(\theta_w) - 0.064 \exp(\rho_d), & T \geq 0^\circ\text{C} \\ 5.507 - 6.777 \exp(\%_{\text{clay}}) + 1.444 \exp(\theta_{\text{tot}}), & -2.5^\circ\text{C} \leq T < 0^\circ\text{C} \\ 0.005 - 14.103(\%_{\text{clay}}) + 2.594 \theta_{\text{tot}}, & T < -2.5^\circ\text{C} \end{cases} \quad (12)$$

where θ_{tot} is the total water content under the negative temperature, which means the sum content of moisture content (θ_w) and solid ice content, and $\%_{\text{clay}}$ is the soil clay content.

Hence, based on the studies of Johansen (1975) and Du et al. (2022) and the new K_e model, a new model for STC has been proposed. The λ_{sat} scheme was proposed by Johansen (1975). Additionally, Du et al. (2022) developed a new

model for λ_{dry} with different calculation methods under a demarcation point of $\rho_d = 1.4 \text{ gcm}^{-3}$. The new STC model was established as follows:

$$\lambda = \begin{cases} (\lambda_{\text{sat}} - \lambda_{\text{dry}})K_e + \lambda_{\text{dry}} & S_r > 1 \times 10^{-5} \\ \lambda_{\text{dry}} & S_r \leq 1 \times 10^{-5} \end{cases} \quad (13)$$

$$\lambda_{\text{sat}} = \begin{cases} \lambda_s^{1-\theta_{\text{sat}}} \lambda_w^{\theta_{\text{sat}}}, & T \geq 0^\circ\text{C} \\ \lambda_s^{1-\theta_{\text{sat}}} \lambda_w^{\theta_w} \lambda_{\text{ice}}^{\theta_{\text{sat}} - \theta_w}, & T < 0^\circ\text{C} \end{cases} \quad (\text{Johansen, 1975}) \quad (14)$$

$$\lambda_{\text{dry}} = \begin{cases} \exp(-1.432/\rho_d - 0.494), & \rho_d < 1.4 \text{ gcm}^{-3} \\ \frac{(\kappa_s \lambda_s - \lambda_a) \rho_d + \lambda_a \rho_s}{\rho_s - (1 - \kappa_s) \rho_d}, & \rho_d \geq 1.4 \text{ gcm}^{-3} \end{cases} \quad (\text{Du et al., 2022}) \quad (15)$$

$$K_e = \begin{cases} 0.173 + 0.544 \exp(\theta_w) - 0.064 \exp(\rho_d), & T \geq 0^\circ\text{C} \\ 5.507 - 6.777 \exp(\%_{\text{clay}}) + 1.444 \exp(\theta_{\text{tot}}), & -2.5^\circ\text{C} \leq T < 0^\circ\text{C} \\ 0.005 - 14.103(\%_{\text{clay}}) + 2.594 \theta_{\text{tot}}, & T < -2.5^\circ\text{C} \end{cases} \quad (16)$$

3.2 Validation of the new model for STC

Figure 5 compares the measurements and estimates by the previous models and the new STC model in the testing portion, and Table 4 shows the performance metrics for each model. The results showed that the new model produced the most accurate predictions, with only a slight underestimation. At 10 cm depth, the C&K model resulted in best predictions, followed by Campbell model and the new model. At

20 cm depth, the new model had the smallest RMSE, MAE, and MBE. And at the depth of 50 cm, the errors of the new model were significantly reduced than those in other models.

To further ascertain the relative performance of the above models over different temperature ranges, the mean values of the models were calculated at depths of 10–50 cm, and then, the values of RMSE and R^2 were given (Fig. 6). The results showed that the RMSE value of the new model was the smallest over any temperature range, which means a

Table 3 Errors of the K_e parameter of the fitting group under different influencing factors

Temperature range	Sequence number	Independent variable	R^2	Estimated error
$\geq 0^\circ\text{C}$	1	θ_w	0.229	0.117
	2	θ_w and ρ_d	0.341	0.109
	3	θ_w , ρ_d , and $\%_{\text{clay}}$	0.342	0.108
$-2.5 \sim 0^\circ\text{C}$	1	θ_{tot}	0.755	0.112
	2	θ_{tot} and $\%_{\text{clay}}$	0.762	0.110
	3	θ_{tot} , $\%_{\text{clay}}$, and ρ_d	0.762	0.111
$< -2.5^\circ\text{C}$	1	θ_{tot}	0.828	0.103
	2	θ_{tot} and $\%_{\text{clay}}$	0.845	0.098
	3	θ_{tot} , $\%_{\text{clay}}$, and ρ_d	0.845	0.098

θ_{tot} is the total water content under the negative temperature, which means the sum content of moisture content (θ_w) and solid ice content, ρ_d means the soil dry density, and $\%_{\text{clay}}$ is the soil clay content

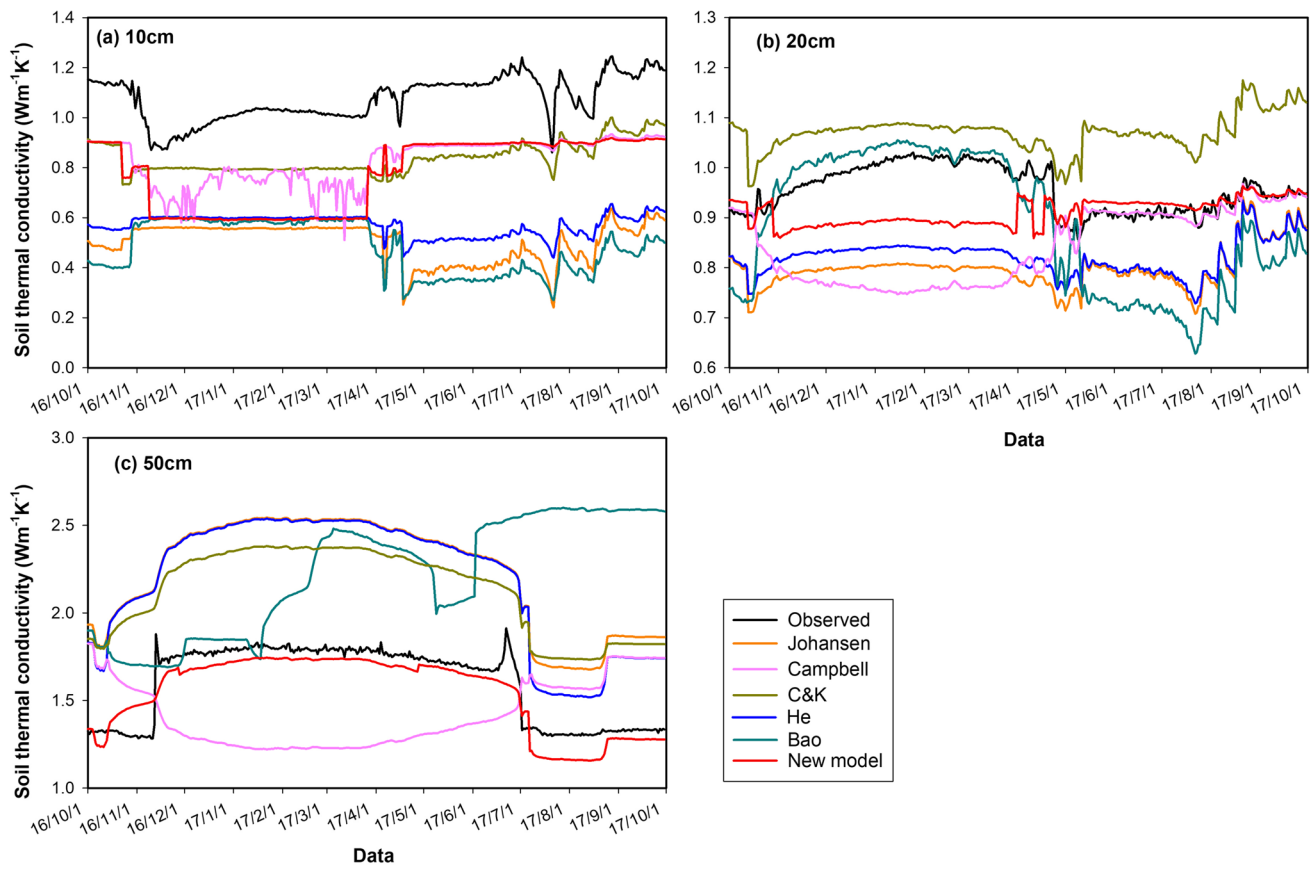


Fig. 5 Comparison of the estimated STC with the measured values at depth of 10–50 cm in the testing portion

Table 4 The error values of the estimated STC by different models of the testing portion

Site	Metric	Johansen model	Campbell model	C&K model	He model	Bao model	New model
10 cm	RMSE	0.589	0.255	0.247	0.518	0.622	0.316
	MAE	0.574	0.249	0.239	0.507	0.598	0.304
	R^2	0.069	0.698	0.507	0.066	0.360	0.640
	MBE	-0.574	-0.249	-0.239	-0.507	-0.598	-0.303
20 cm	RMSE	0.167	0.161	0.124	0.141	0.119	0.078
	MAE	0.158	0.118	0.115	0.135	0.092	0.061
	R^2	0.072	0.589	0.125	0.322	0.773	0.209
	MBE	-0.158	-0.11	0.115	-0.135	-0.070	-0.046
50 cm	RMSE	0.643	0.436	0.533	0.616	0.757	0.097
	MAE	0.630	0.419	0.527	0.589	0.622	0.084
	R^2	0.885	0.861	0.906	0.859	0.062	0.871
	MBE	0.630	-0.179	0.527	0.589	0.615	-0.057

Bold data represents the best result for each statistic

significant improvement compared with other models. Furthermore, the R^2 of the new model was best in the range of $-2.5 \sim 0 \text{ }^\circ\text{C}$ and also ranked well in other temperature ranges. In other words, the new model with demarcation

points of $0 \text{ }^\circ\text{C}$ and $-2.5 \text{ }^\circ\text{C}$ achieved the best fit within a wide temperature range. Thus, the new model could reflect changes in the STC at depths of 10–50 cm in permafrost regions with favorable simulation performance.

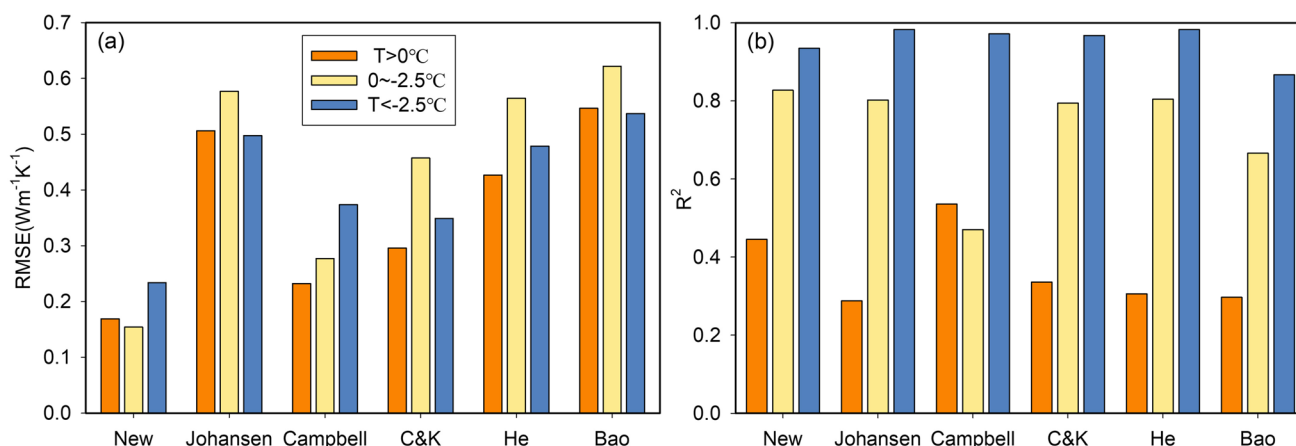


Fig. 6 RMSE (a) and R^2 (b) of different STC models under different ranges of soil temperature

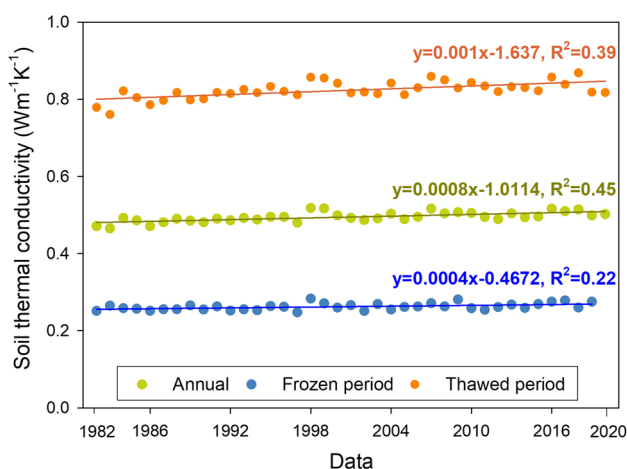


Fig. 7 Interannual variation features of STC over the permafrost region on QTP during 1982–2020

3.3 Temporal and spatial characteristics of STC in the permafrost region of the QTP

Based on the new model, the daily STC product in the permafrost region of the QTP at the depths of 0–28 cm was estimated by combining the ERA5 product and the GSDE dataset. Then, the temporal and spatial characteristics of STC in the permafrost region from 1982 to 2020 were analyzed. Note that the ERA5 product used ended on December 31, 2020. Thus, the research stage of the frozen period runs until 2019, which was the period from October 1, 2019, to April 30, 2020.

As illustrated in Fig. 7, the average STC value of the permafrost was about $0.495 \text{ Wm}^{-1}\text{K}^{-1}$, and those in the frozen

period (from October of that year to April of the following year) and thawed period (from May to September) were $0.262 \text{ Wm}^{-1}\text{K}^{-1}$ and $0.823 \text{ Wm}^{-1}\text{K}^{-1}$, respectively. In recent 39 years, the interannual variation of STC in the permafrost region of QTP showed a tiny increasing trend, which was the same in both the thawed and frozen periods. Overall, the STC in the permafrost region of the QTP increased slowly from 1982 to 2020.

Figure 8 shows the spatial characteristics of the STC in the permafrost region of the QTP. Geographically, the STC was high in the southeast and low in the northwest (Fig. 8a). In general, the lower values occurred in high-altitude mountains, which have lower mean annual ground temperatures (MAGTs) (Ni et al. 2020). As illustrated in Fig. 8b and c, on the whole, in both frozen or thawed periods, STC values were high in the southeast and low in the northwest. Specifically, the STC values were concentrated in the $0.2 \sim 0.3 \text{ Wm}^{-1}\text{K}^{-1}$ range during the frozen period, with little spatial difference. High values of STC were found in the eastern and southeastern regions where with relatively high θ_w . In contrast, during the thawed period, the STC values were concentrated in the 0.6 to $1.0 \text{ Wm}^{-1}\text{K}^{-1}$ range, with a large spatial spread and scatter, which was related to the spatial spread of precipitation. The differences in spatial distributions of STC in the permafrost regions of the QTP are the result of climate, soil temperature, θ_w , vegetation type, soil texture, and other factors. First, from east to west, the climate of the QTP gradually changes from sub-humid to extremely arid, with large variations. According to Yu et al. (2015), the high summer temperature values of the QTP usually occur in the southwest, southeast, and northeast regions of the QTP. Additionally, the θ_w in the permafrost region of the QTP is

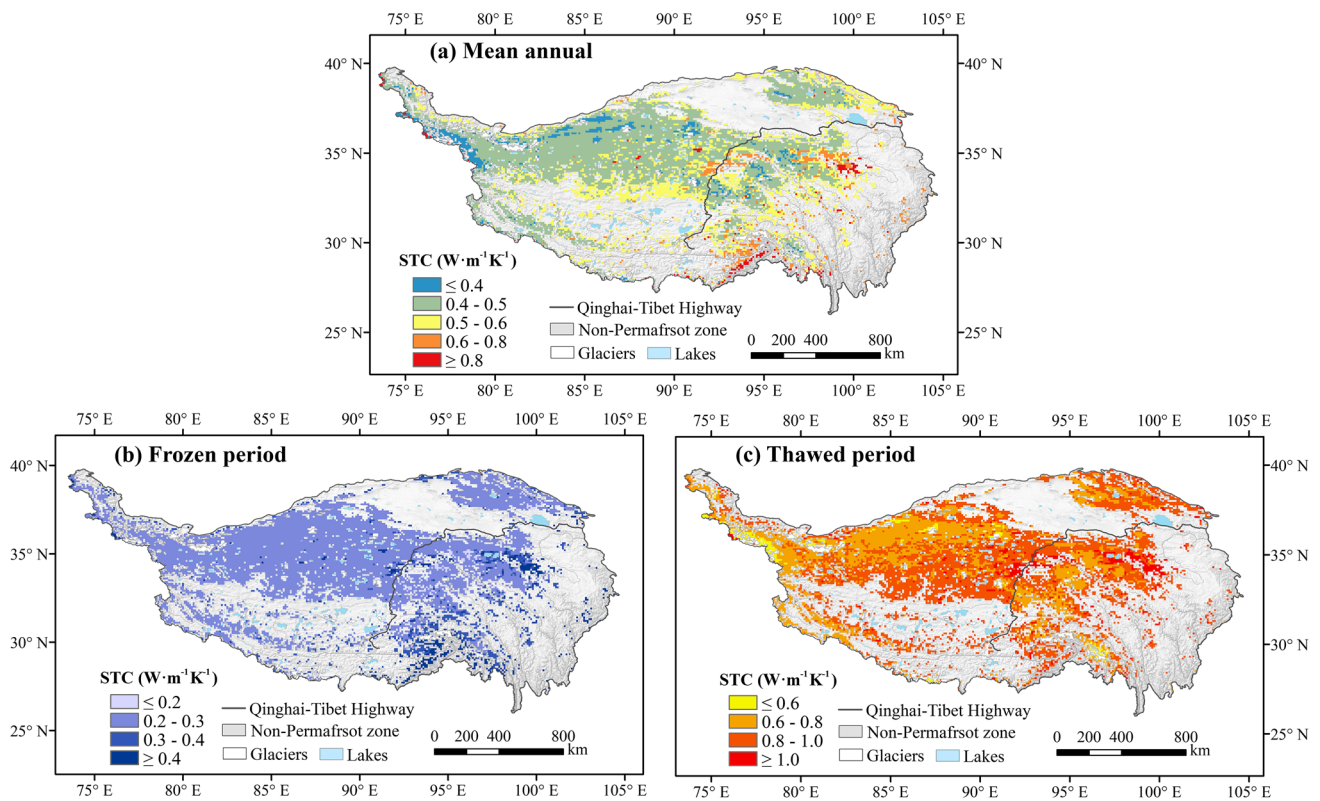


Fig. 8 Spatial distribution of STC across the permafrost regions on the QTP from 1982 to 2020. **a** Mean annual. **b** Frozen period. **c** Thawed period

higher in the southeast, but lower in the southwest and hinterland due to the spatial distribution of precipitation (Zhao et al. 2019c). This results in a better ecological environment and higher vegetation coverage in the eastern part of the QTP (Yang et al. 2009). On the contrary, the western part's ecological environment is poor and its vegetation coverage is low (Wang et al. 2016). Generally speaking, well-developed vegetation can effectively increase soil moisture and organic matter content (Hu et al. 2022), further improving STC. In addition, a previous study found that the degree of soil development and the number of soil types were higher in the eastern part of the QTP than in the western part (Li et al. 2015). All these factors may lead to significant spatial differences in the STC. Our evaluation results in the permafrost region in the QTP differ slightly from previous results (Liu et al. 2023) during the frozen period. There are two reasons for these differences: (1) Our results are for the top 28 cm of soil, while Liu's results are for the top 5 cm. (2) Our results are mainly calculated from parameterization model developed by the measured data, while those of Liu et al. (2023) are from XGBoost (a machine learning model). Moreover, there are some errors and differences in the results caused

by different input data including some known errors in our data results, which are analyzed in Section 3.4.

Figure 9 shows the spatial distribution of the mean STC in the permafrost region of the QTP from 1982 to 2020. From December to the following March, the soil was in the fully frozen stage, and the STC at this stage was essentially the same. After April, the STC in the boundary region of the permafrost began to rise, as the frozen soil began to thaw due to rising air temperatures (Fig. 13). In May, further increases in air temperature, with associated increases in precipitation from the onset of the summer monsoon (Zhang et al. 2017b), led to an increase in the θ_w , followed by an increase in STC, especially in the transition zone of the permafrost region and the seasonal permafrost region. It was found that the average annual ground temperature of the permafrost in this area was often close to 0 °C. This type of permafrost was extremely sensitive to climate change and was frequently the main constituent of the permafrost degradation areas (Ni et al. 2020). From June to August, the plateau experiences its maximum air temperature and precipitation (Fig. 13). The soil in the permafrost region thawed completely, and in addition, the surface solar radiation, θ_w , and soil temperature

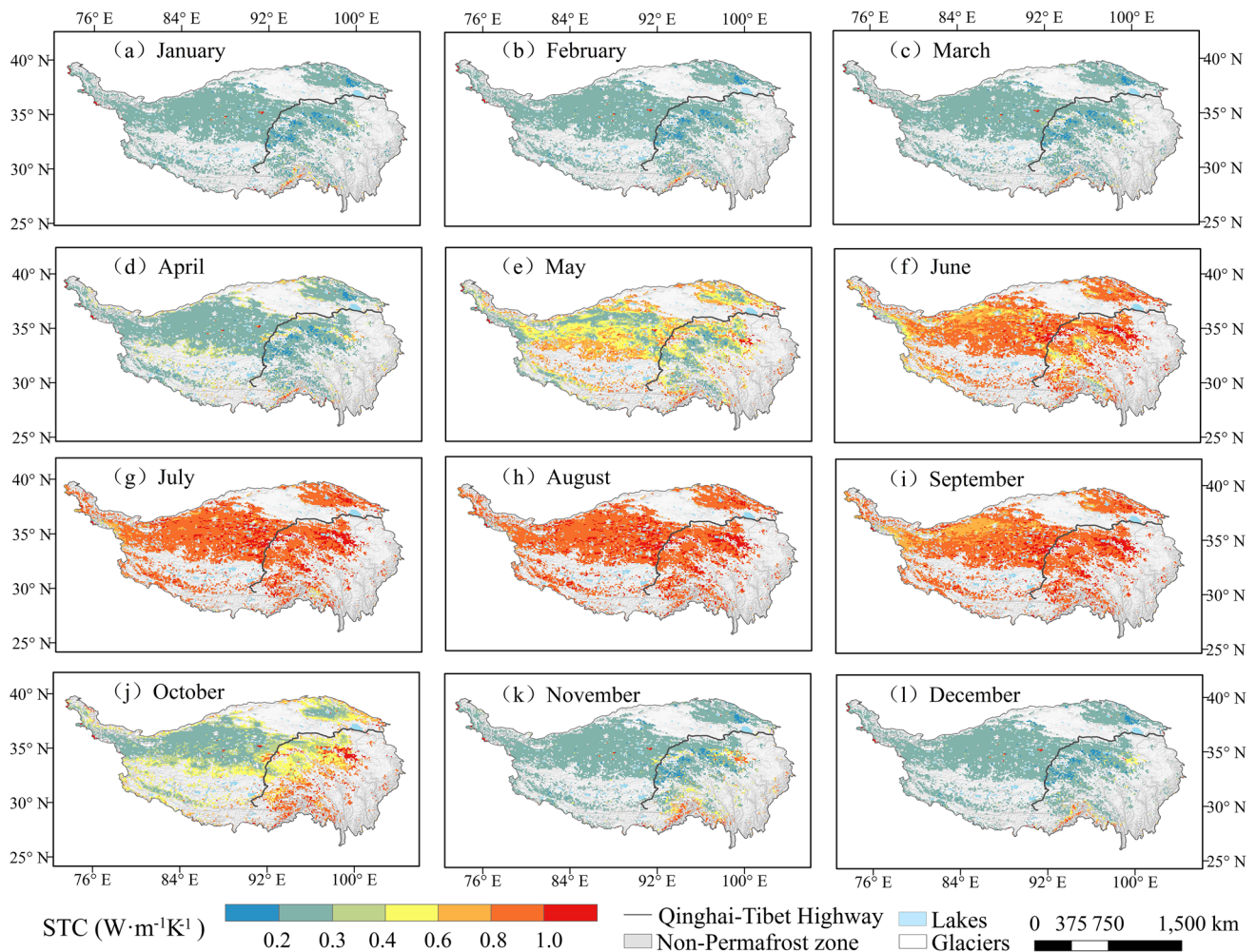


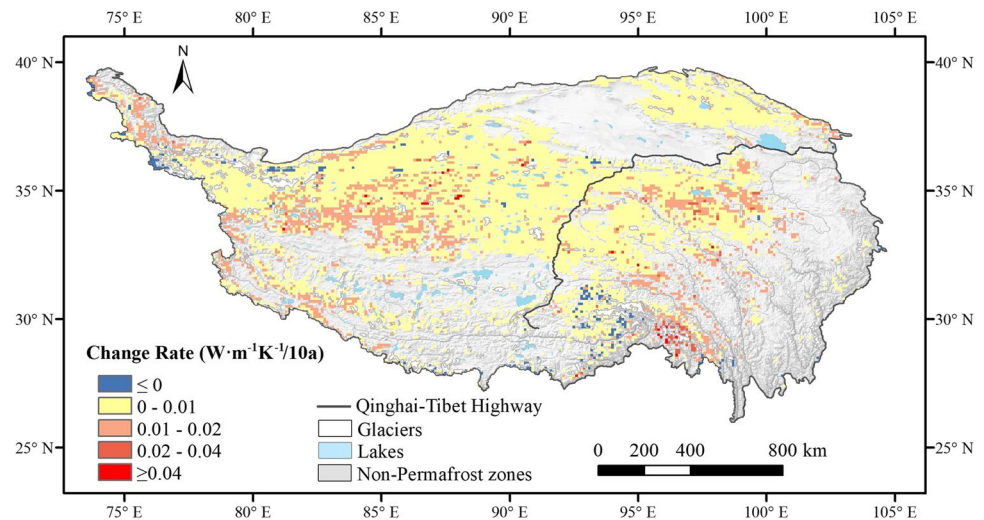
Fig. 9 Monthly spatial distribution of STC over the permafrost on the QTP from 1982 to 2020

were large. In August, the STC in the permafrost region reached its yearly maximum. Notably, large values of STC appeared in the southeastern part of the QTP, mainly due to higher precipitation in this region under the influence of abundant water vapor from the Indian Ocean and the Bay of Bengal (Feng and Zhou 2012). In September, the summer monsoon gradually slowed and precipitation gradually decreased from the northwest to the southeast; the STC also decreased following the same pattern. Beginning in October, the air temperature began to drop, and the soil temperature fell accordingly. As liquid water turns into solid ice, the soil begins to freeze. The STC started to decrease first in the hinterland of the QTP. By November, the soil was almost fully frozen in most areas, except for the high θ_w areas in the southern area, and the STC values mostly began to stabilize. In general, as the temperature increased, the STC in the permafrost region of the QTP increased from the permafrost boundary region to the central region and from the southeast

to the northwest and then decreased in the opposite direction as the temperature decreased.

Previous studies have pointed out that the variation of soil thermal properties (STC, soil heat capacity, etc.) and the heat conversion during the ice-water phase transition may cause abnormal soil temperature fluctuations (Yang and Wang 2019) and further affect the stability of the permafrost (Ni et al. 2022). Figure 10 shows the spatial change rate of the STC in the permafrost region from 1982 to 2020. We can see that the annual change rates were positive, except for in some sporadic areas. In other words, the STC in the permafrost region of the QTP mainly showed a consistent increasing trend, but the overall change was slight ($0.008 \text{ Wm}^{-1}\text{K}^{-1}/10\text{a}$). It is noteworthy that STC increased rapidly in the southwest of the QTP, where annual average values increased in the range of $0.01 \sim 0.03 \text{ Wm}^{-1}\text{K}^{-1}/10\text{a}$, which might be related to its higher rate of temperature rise (Ran et al. 2018) and greater increasing trend in θ_w (Zhao et al. 2019c).

Fig. 10 Change rate of the STC across the permafrost regions on the QTP from 1982 to 2020



Based on the mean annual ground temperature (MAGT) and GIPL2 model, permafrost areas on the QTP were generally divided into six types: extremely unstable permafrost, unstable permafrost, transition permafrost, sub-stable permafrost, stable permafrost, and extremely stable permafrost (Cheng and Wang 1982; Qin et al. 2017) (Fig. 13). Combined with the permafrost type, we can see that the higher STC values are typically distributed in the transition region between permafrost and seasonally frozen ground (Fig. 8), which belongs to the unstable permafrost type in danger of thaw settlement (Ni et al. 2022). Areas showing decreasing trend in STC were roughly distributed in sporadic regions along the north-western and southeastern margins (Fig. 10), most of which were considered extremely stable permafrost, and the rate of change in these areas was between -0.033 and $0 \text{ Wm}^{-1}\text{K}^{-1}/10\text{a}$. Permafrost with STC increasing rates between 0 and $0.01 \text{ Wm}^{-1}\text{K}^{-1}/10\text{a}$ was mostly identified as stable permafrost and sub-stable permafrost. Regions with relatively rapid STC growth rates were concentrated in the eastern, southeastern, and south-western regions and were mostly considered unstable and extremely unstable permafrost. As we all know, under the continued warming of the QTP, the increase of soil temperature and the drastic phase transition of the ice-water causing increase in STC. Higher STC would entail more heat entering the ground and hasten permafrost degradation (Mekonnen et al. 2021). This confirms the reliability of our simulation results to some extent. However, the factors causing permafrost degradation are very complex (Chang et al. 2022; Ding et al. 2019; Guo and Wang 2017; Li et al. 2021), and the specific degradation mechanism needs to be further studied. Overall, the spatial features of the rates of STC change in the permafrost regions of the QTP over the past 40 years showed significant increases in the southeastern, eastern, and south-western parts; a slight increase in the hinterland; and a significant decrease along the north-western margin.

3.4 Possible causes for simulation STC in the permafrost region of the QTP

To assess the accuracy of the estimated STC product, we compared them with the observed data along the Qinghai-Tibet Highway (Fig. 11). As shown in Fig. 11, when the soil temperature was above $0 \text{ }^\circ\text{C}$, the calculated STC corresponded nicely with the observed value, with a 13.8% error. However, at negative soil temperatures, the new model gave significantly lower STC values compared to those of the observations, resulting in 366.9% error. Farouki (1981) estimated that reasonable predictions were those that do not deviate more than about 25% from measured values. In other words, the calculated STC data based on the new model and the ERA5 data in the permafrost region of the QTP were feasible during the thawed period. Possible causes of the simulation errors are discussed below.

3.4.1 The influence of the input data

The establishment of the new model was based on observations from field stations, ensuring both the reliability and continuity of the data. However, when developing the STC product in the permafrost regions of QTP, soil temperature and water data from ERA5 data and the soil data of GSDE were used as substitutes for input data due to the lack of field observation data.

There have been numerous studies on the applicability of ERA5 data to the QTP. Yang et al. (2020) pointed out that the soil temperature and water data from ERA5 performed well on the QTP during the thawed period. Figure 12 shows the variations in the observed θ_w and those calculated from ERA5 data at temperatures below $0 \text{ }^\circ\text{C}$ at the XDT site. The difference between the calculated values and the observed

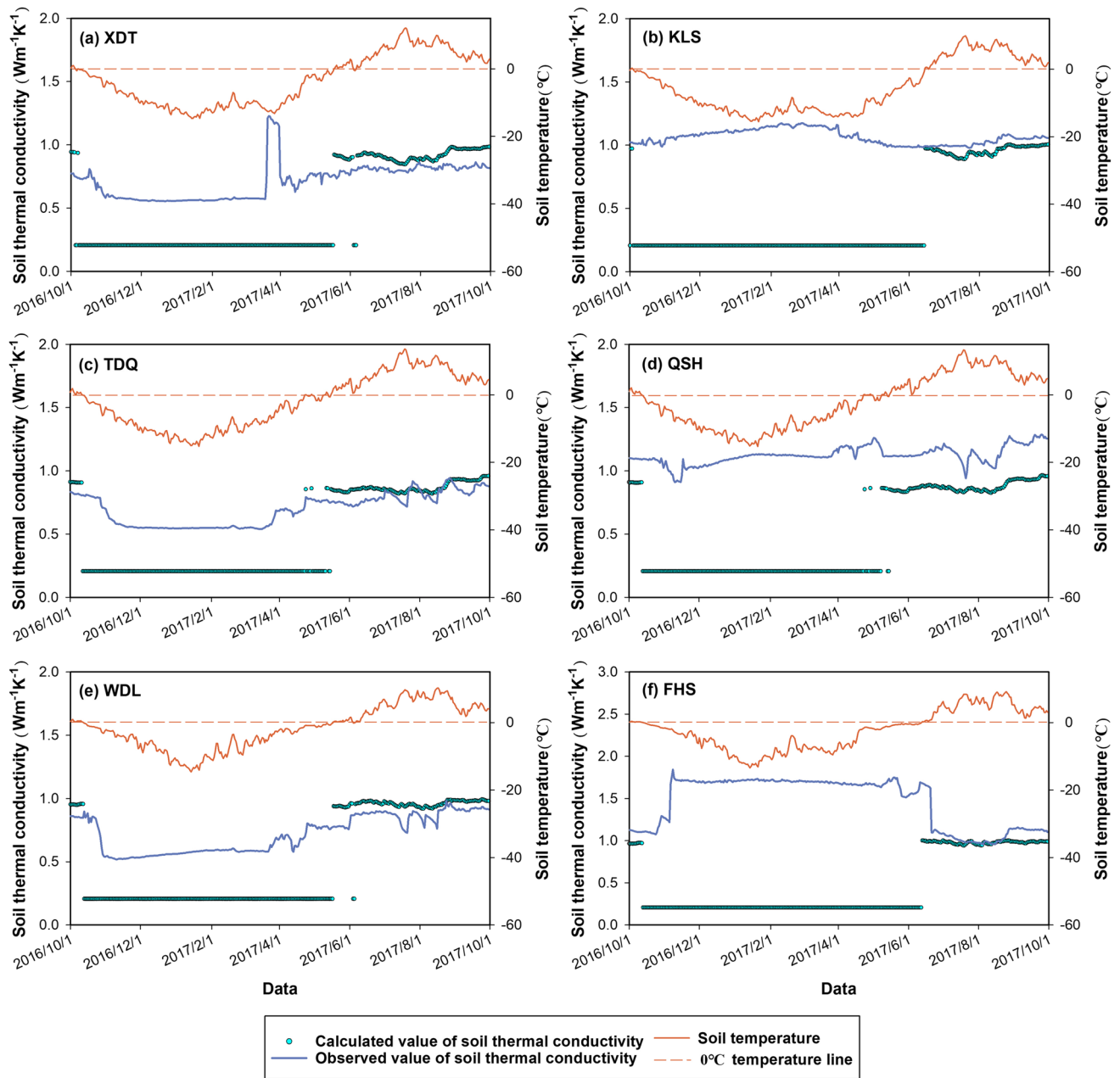


Fig. 11 Comparison between STC values of observed and estimated along the Qinghai-Tibet Highway from October 1, 2016, to September 30, 2017

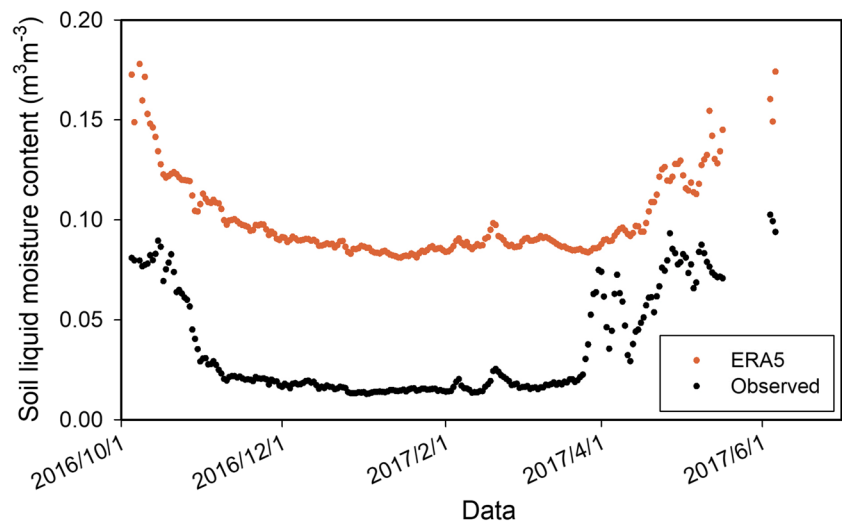
values was large, with a clear overestimation. This inaccuracy also occurred at several other sites in this study and inevitably weakens the contribution of the ice content and the phase transition to the STC. This may be one of the main reasons for the underestimated values of the STC in the permafrost regions of the QTP during the frozen period.

In addition, there are some errors between the soil texture derived from the GSDE dataset by Shangguan et al. (2013) and the observed reality. Yang et al. (2020) compared this dataset and the laboratory measurements along the

Qinghai-Tibet Highway and found that the GSDE overestimated the clay content and underestimated the sand content, which enhanced the water retention capacity of the soil and thus increased the θ_w . This would also increase the calculation error of the new model.

In summary, the quality of the STC product performed better during the thawed period than that during the frozen period. In the future, with the improvement of the accuracy of the input dataset, the accuracy of the STC product will be also improved.

Fig. 12 Variations in the soil moisture content of observed and estimated by ERA5 below 0 °C at XDT site from October 1, 2016, to September 30, 2017



3.4.2 The shortcomings of the new model

There are many factors affecting STC, such as θ_w , ice content, soil temperature, soil texture, organic matter content, salinity, and vegetation type (He et al. 2019; 2021b; Malek et al. 2021; Nikoosokhan et al. 2016). The improved model in this study considered primarily mineral soil, but delegated the effects of soil organic matter, gravel fraction, soil salinity, or other factors. For example, the salinity affects the freezing temperature of liquid water and then affects the variation of STC through soil temperature and θ_w . Moreover, soil organic matter affects the bulk density of the soil and the thermal resistance between particles, resulting in changes in soil porosity, θ_w and other factors that have a great impact on STC. Hence, the inclusion of more influential factors in the calculation model may increase its reliability.

The choice of -2.5 °C as a universal threshold may not be appropriate for all soil types, particularly given substantial variations in soil freezing characteristic curves between fine and coarse soils (Hu et al. 2020b; Teng et al. 2020). The soil types and other soil properties in the permafrost region of the QTP are not entirely consistent. Liu et al. (2022) indicated that the soil particles of the QTP are dominated by sand, especially in the northwest portion; the southeastern QTP has a high content of silt and clay. In this study, the soil particles of the soil samples from the Qinghai-Tibet Highway are mainly sand content, with an average content of 93%. That is, our new model is suitable for predicting STC for coarse soils. This might bring some calculation errors to the simulation of STC in the southeastern QTP. Hence, establishing different temperature nodes for different soil types should be further studied in future works.

4 Conclusions

This study divided three temperature range to develop a new STC model in the permafrost region of the QTP. Based on the new model, the daily STC product over the permafrost region of the QTP from 1982 to 2020 was estimated. The main conclusions were as follows:

1. In the temperature range of -2.5 to 0 °C, the moisture undergoes a rapid phase change with slight changes in soil temperature. When the temperature was below -2.5 °C, the moisture content remains basically unchanged; even if the temperature changes greatly, it changes smoothly.
2. The simulation accuracy of the new model had been improved in permafrost regions, and it could better reflect the changing properties of the STC, especially for soils of the 50 cm depth.
3. The average value of the STC in the permafrost regions on the QTP was about $0.495 \text{ Wm}^{-1}\text{K}^{-1}$ during 1982 to 2020, showing a spatial pattern of low STCs in the northwest and high STCs in the southeast.
4. From 1982 to 2020, the STC showed a relatively slow increasing trend with a change rate of $0.008 \text{ Wm}^{-1}\text{K}^{-1}/10\text{a}$. Spatially, the regions with the highest rates of increase were concentrated in the east, southeast, and south-west and included mostly unstable or extremely unstable permafrost.
5. The quality of the STC product performed better during the thawed period than that during the frozen period. In the future, with the improvement of the accuracy of the input dataset (e.g., soil moisture content, soil texture), the accuracy of the STC product will be also improved.

Appendix

Fig. 13 Monthly air temperature and precipitation over the permafrost on the QTP

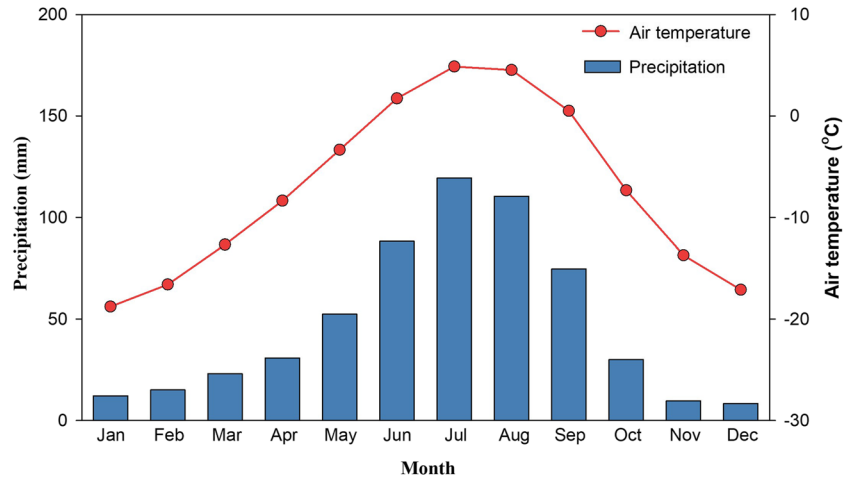
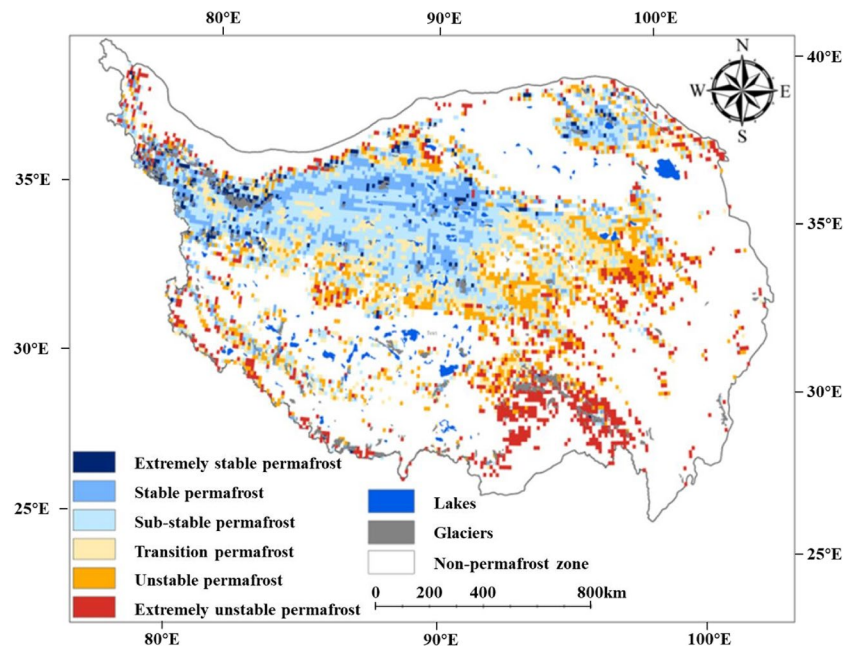


Fig. 14 Distributions of the permafrost types (Qin et al. 2017)



Author contributions All authors contributed to the study conception and design. Yizhen Du and Jie Ni wrote the main manuscript text. Ren Li, Tonghua Wu, and Guojie Hu collected data and analysis the data. ShuhuaYang and Xuefei Weng prepared figures. All authors read and approved the final.

Funding This work was supported by the National Natural Science Foundation of China (42071093), the State Key Laboratory of Cryospheric Science (SKLCS-OP-2021-04), the Natural Science Foundation of Shandong Province (ZR2022QD044), the National Natural Science Foundation of China (41671070), the State Key Laboratory of Cryospheric Science (SKLCS-ZZ-2023), and the Natural Science Foundation of Shandong Province (ZR2022QD016).

Data availability No datasets were generated or analysed during the current study.

Declarations

Competing interests The authors declare no competing interests.

References

- Ballard V, Arp PA (2005) Modeling soil thermal conductivities over a wide range of conditions. *J Environ Eng Sci* 4(6):549–558. <https://doi.org/10.1139/s05-007>
- Bao H, Koike T, Yang K, Wang L, Shrestha M, Lawford P (2016) Development of an enthalpy-based frozen soil model and its validation in a cold region in China. *J Geophys Res: Atmos* 121(10):5259–5280. <https://doi.org/10.1002/2015JD024451>
- Campbell GS (1985) Soil physics with BASIC: Transport Models for Soil-Plant Systems. *Developments in Soil Science*, vol 14. Elsevier, New York, p 14
- Campbell GS, Jungbauer JD, Bidlake WR, Hungerford RD (1994) Predicting the effect of temperature on soil thermal conductivity. *Soil Sci* 158(5):307–313
- Chang Z, Qi P, Zhang G, Sun Y, Tang X, Jiang M et al (2022) Latitudinal characteristics of frozen soil degradation and their response to climate change in a high-latitude water tower. *Catena* 214:106272. <https://doi.org/10.1016/j.catena.2022.106272>
- Chen L, Yu W, Lu Y, Wu P, Han F (2021) Characteristics of heat fluxes of an oil pipeline armed with thermosyphons in permafrost regions. *Appl Therm Eng* 190:116694. <https://doi.org/10.1016/j.applthermaleng.2021.116694>
- Cheng G, Wang S (1982) On the zonation of high-altitude permafrost in China. *J Glaciol Geocryol* 4(2):1–17 ((in Chinese))
- Cheng M, Zhong L, Ma Y, Zou M, Ge N, Wang X, Hu Y (2019) A study on the assessment of multi-source satellite soil moisture products and reanalysis data for the Tibetan Plateau. *Remote Sensing* 11(10):1196. <https://doi.org/10.3390/rs11101196>
- Côté J, Konrad J (2005) A generalized thermal conductivity model for soils and construction materials. *Can Geotech J* 42(2):443–458. <https://doi.org/10.1139/t04-106>
- Cui F, Liu Z, Chen J, Dong Y, Jin L, Peng H (2020) Experimental test and prediction model of soil thermal conductivity in permafrost regions. *Appl Sci* 10(7):2476. <https://doi.org/10.3390/app10072476>
- Czernecki B, Taszarek M, Marosz M, Pótrolniczak M, Kolendowicz L, Wyszogrodzki A, Szturc J (2019) Application of machine learning to large hail prediction-the importance of radar reflectivity, lightning occurrence and convective parameters derived from ERA5. *Atmos Res* 227:249–262. <https://doi.org/10.1016/j.atmosres.2019.05.010>
- Dai Y, Wei N, Yuan H, Zhang S, Shangguan W, Liu S, Lu X, Xin Y (2019) Evaluation of soil thermal conductivity schemes for use in land surface modeling. *J Adv Model Earth Syst* 11(11):3454–3473. <https://doi.org/10.1029/2019MS001723>
- De Vries DA (1963) Thermal properties of soils. In: van Dijk WR (ed) *Physics of Plant Environment*. North Holland Publishing, Amsterdam, pp 210–235
- Dee DP, Uppala SM, Simmons AJ, Berrisford P, Poli P, Kobayashi S et al (2011) The ERA-Interim reanalysis: configuration and performance of the data assimilation system. *Q J R Meteorol Soc* 137(656):553–597. <https://doi.org/10.1002/qj.828>
- Ding Y, Zhang S, Zhao L, Li Z, Kang S (2019) Global warming weakening the inherent stability of glaciers and permafrost. *Sci Bull* 64(4):245–253. <https://doi.org/10.1016/j.scib.2018.12.028>
- Dong J, Li X, Han B et al (2022) A regional study of in-situ thermal conductivity of soil based on artificial neural network model. *Energy Build* 257:111785. <https://doi.org/10.1016/j.enbuild.2021.111785>
- Du Y, Li R, Zhao L, Yang C, Wu T, Hu G, Xiao Y, Zhu X, Yang S, Ni J, Ma J (2020) Evaluation of 11 soil thermal conductivity schemes for the permafrost region of the central Qinghai-Tibet Plateau. *Catena* 193:104608. <https://doi.org/10.1016/j.catena.2020.104608>
- Du Y, Li R, Wu T, Yang C, Zhao L, Hu G, Xiao Y, Yang S, Ni J, Ma J, Shi J, Qiao Y (2022) A new model for predicting soil thermal conductivity for dry soils. *Int J Therm Sci* 176:107487. <https://doi.org/10.1016/j.ijthermalsci.2022.107487>
- Duan Z, Dong C, Yan X, Sun Q, Li B (2022) Experimental research of fracture damage behavior of loess with different prefabricated cracks. *Eng Fract Mech* 275:108849. <https://doi.org/10.1016/j.engfractmech.2022.108849>
- Duan Z, Yan X, Sun Q, Tan X, Chen X (2021) New models for calculating the electrical resistivity of loess affected by moisture content and NaCl concentration. *Environ Sci Pollut Res* 1–15. <https://doi.org/10.1007/s11356-021-16971-z>
- Farouki OT (1981) Thermal properties of soils. U.S. Army Corps of Engineers, Cold Regions Research and Engineering Laboratory, Hanover, NH
- Feng L, Zhou T (2012) Water vapor transport for summer precipitation over the Tibetan Plateau: multidata set analysis. *J Geophys Res Atmos* 117(D20). <https://doi.org/10.1029/2011JD017012>
- Guo D, Wang H (2017) Permafrost degradation and associated ground settlement estimation under 2 C global warming. *Clim Dyn* 49:2569–2583. <https://doi.org/10.1007/s00382-016-3469-9>
- He H, Zhao Y, Dyck MF, Si B, Jin H, Lv J, Wang J (2017) A modified normalized model for predicting effective soil thermal conductivity. *Acta Geotech* 12(6):1281–1300. <https://doi.org/10.1007/s11440-017-0563-z>
- He H, Noborio K, Johansen Ø, Dyck MF, Lv J (2019) Normalized concept for modelling effective soil thermal conductivity from dryness to saturation. *Eur J Soil Sci*. <https://doi.org/10.1111/ejss.12820>
- He H, Flerchinger GN, Kojima Y, Dyck M, Lv J (2021a) A review and evaluation of 39 thermal conductivity models for frozen soils. *Geoderma* 382:114694. <https://doi.org/10.1016/j.geoderma.2020.114694>
- He H, Flerchinger GN, Kojima Y, He D, Hardegree SP, Dyck MF, Horton R, Wu Q, Si B, Lv J, Wang J (2021b) Evaluation of 14 frozen soil thermal conductivity models with observations and SHAW model simulations. *Geoderma* 403:115207. <https://doi.org/10.1016/j.geoderma.2021.115207>
- Hersbach H, Bell B, Berrisford P, Horányi A, Sabater M, Nicolas J, Radu R, Schepers D, Simmons A, Soci C, Dee D (2019) Global reanalysis: goodbye ERAInterim, hello ERA5. *ECMWF Newsl* 159:17–24
- Hjort J, Streltsekiy D, Doré G, Wu Q, Bjella K, Luoto M (2022) Impacts of permafrost degradation on infrastructure. *Nat Rev Earth Environ* 3(1):24–38

- Hori M, Sugiura K, Kobayashi K, Aoki T, Tanikawa T, Kuchiki K, Niwano M, Enomoto H (2017) A 38-year (1978–2015) Northern Hemisphere daily snow cover extent product derived using consistent objective criteria from satellite-borne optical sensors. *Remote Sens Environ* 191:402–418. <https://doi.org/10.1016/j.rse.2017.01.023>
- Hu G, Zhao L, Li R, Wu X, Wu T, Xie C, Zhu X, Hao J (2020a) Thermal properties of active layer in permafrost regions with different vegetation types on the Qinghai-Tibetan Plateau. *Theor Appl Climatol*. <https://doi.org/10.1007/s00704-019-03008-2>
- Hu G, Zhao L, Zhu X, Wu X, Wu T, Li R, Xie C, Hao J (2020b) Review of algorithms and parameterizations to determine unfrozen water content in frozen soil. *Geoderma* 368:114277. <https://doi.org/10.1016/j.geoderma.2020.114277>
- Hu Y, Wang G, Du H, Liang S, Luo Y, Dong G, Peng H (2022) Changes in surface soil moisture during freeze-thaw process under different vegetated status using Sentinel-1A in Beiluhe. *J Glaciol Geocryol* 44(6):1925–1934 ((in Chinese))
- Hu G, Zhao L, Li R, Wu X, Wu T, Zou D et al (2023) Dynamics of the freeze–thaw front of active layer on the Qinghai-Tibet Plateau. *Geoderma* 430:116353. <https://doi.org/10.1016/j.geoderma.2023.116353>
- Inaba H (1983) Experimental study on thermal properties of frozen soils. *Cold Reg Sci Technol* 8(2):181–187
- Johansen O (1975) *Varmeledningsevne av jordarter* (Thermal conductivity of soils), University of Trondheim, Trondheim, Norway., US Army Corps of Engineers, Cold Regions Research and Engineering Laboratory, Hanover, N.H. CRREL Draft English Translation 637
- Kersten M (1949) Thermal properties of soils. Minnesota University Institute of Technology, Minneapolis, MN
- Kojima Y, Heitman JL, Flerchinger GN, Ren T, Horton R (2016) Sensible heat balance estimates of transient soil ice contents. *Vadose Zone J* 15(5):0. <https://doi.org/10.2136/vzj2015.10.0134>
- Li W, Zhao L, Wu X, Zhao Y, Fang H, Shi W (2015) Distribution of soils and landform relationships in the permafrost regions of the Qinghai-Xizang (Tibetan) Plateau. *Chin Sci Bull* 60:2216–2226. <https://doi.org/10.1360/N972014-01206>. ((in Chinese))
- Li R, Zhao L, Wu T, Wang Q, Ding Y, Yao J, Wu X, Hu G, Xiao Y, Du Y, Zhu X, Qin Y, Yang S, Bai R, Du E, Liu G, Zou D, Qiao Y, Shi J (2019) Soil thermal conductivity and its influencing factors at the Tanggula permafrost region on the Qinghai-Tibet Plateau. *Agric for Meteorol* 264:235–246. <https://doi.org/10.1016/j.agrfo.rmet.2018.10.011>
- Li T, Chen YZ, Han LJ, Cheng LH, Lv YH, Fu BJ et al (2021) Shortened duration and reduced area of frozen soil in the Northern Hemisphere. *Innov* 2(3):100146. <https://doi.org/10.1016/j.xinn.2021.100146>
- Li K, Horton R, He H (2023) Application of machine learning algorithms to model soil thermal diffusivity. *Int Commun Heat Mass Transfer* 149:107092. <https://doi.org/10.1016/j.icheatmasstransfer.2023.107092>
- Lin Z, Wu X (1981) Climatic regionalization of the Qinghai-Tibetan Plateau. *Acta Geogr Sin* 36(1):22–32
- Liu Y, Wu X, Wu T, Zhao L, Li R, Li W et al (2022) Soil texture and its relationship with environmental factors on the Qinghai-Tibet plateau. *Remote Sens* 14(15):3797. <https://doi.org/10.3390/rs14153797>
- Liu W, Li R, Wu T, Shi X, Zhao L, Wu X, Hu G, Yao J, Wang D, Xiao Y, Ma J, Jiao Y, Wang S, Zou D, Zhu X, Chen J, Shi J, Qiao Y (2023) Spatiotemporal patterns and regional differences in soil thermal conductivity on the Qinghai-Tibet Plateau. *Remote Sens* 15:1168. <https://doi.org/10.3390/rs15041168>
- Lu S, Ren T, Gong Y, Horton R (2007) An improved model for predicting soil thermal conductivity from water content at room temperature. *Soil Sci Soc Am J* 71(1):8–14. <https://doi.org/10.2136/sssaj2006.0041>
- Ma W, Ma Y, Su B (2011) Feasibility of retrieving land surface heat fluxes from ASTER data using SEBS: a case study from the NamCo Area of the Tibetan Plateau. *Arct Antarct Alp Res* 43:239–245. <https://doi.org/10.1657/1938-4246-43.2.239>
- Malek K, Malek K, Khanmohammadi F (2021) Response of soil thermal conductivity to various soil properties. *Int Commun Heat Mass Transfer* 127:105516
- Mekonnen ZA, Riley WJ, Grant RF, Romanovsky VE (2021) Changes in precipitation and air temperature contribute comparably to permafrost degradation in a warmer climate. *Environ Res Lett* 16(2):024008. <https://doi.org/10.1088/1748-9326/abc444>
- Mu Y, Ma W, Li G, Mao Y, Liu Y (2020) Long-term thermal and settlement characteristics of air convection embankments with and without adjacent surface water ponding in permafrost regions. *Eng Geol* 266:105464. <https://doi.org/10.1016/j.enggeo.2019.105464>
- Ni J, Wu T, Zhu X, Hu G, Zou D, Wu X, Li R, Xie C, Qiao Y, Pang Q, Hao J, Yang C (2020) Simulation of the present and future projection of permafrost on the Qinghai-Tibet Plateau with statistical and machine learning models. *J Geophys Res: Atmos*. <https://doi.org/10.1029/2020jd033402>
- Ni J, Wu T, Zhu X, Wu X, Pang Q, Zou D, Chen J, Li R, Hu G, Du Y, Hao J, Li X, Qiao Y (2022) Risk assessment of potential thaw settlement hazard in the permafrost regions of Qinghai-Tibet Plateau. *Sci Total Environ* 776:145855. <https://doi.org/10.1016/j.scitotenv.2021.145855>
- Nikolaev I, Leong W, Rosen M (2013) Experimental investigation of soil thermal conductivity over a wide temperature range. *Int J Thermophys* 34(6):1110–1129. <https://doi.org/10.1007/s10765-013-1456-5>
- Nikoosokhan S, Nowamooz H, Chazallon C (2016) Effect of dry density, soil texture and time-spatial variable water content on the soil thermal conductivity. *Geomech Geoen* 11(2):149–158. <https://doi.org/10.1080/17486025.2015.1048313>
- Ochsner T, Baker J (2008) In situ monitoring of soil thermal properties and heat flux during freezing and thawing. *Soil Sci Soc Am J* 72(4):1025
- Ochsner T, Horton R, Ren T (2001) A new perspective on soil thermal properties. *Soil Sci Soc Am J* 65(6):1641–1647. <https://doi.org/10.2136/sssaj2001.1641>
- Pei W, Zhang M, Yan Z, Li S, Lai Y (2019) Numerical evaluation of the cooling performance of a composite L-shaped two-phase closed thermosyphon (LTPCT) technique in permafrost regions. *Sol Energy* 177:22–31. <https://doi.org/10.1016/j.solener.2018.11.001>
- Pei W, Zhang M, Yan Z, Lai Y, Lu J, Dai Y (2022) Thermal control performance of the embankment with L-shaped thermosyphons and insulations along the Gonghe-Yushu Highway. *Cold Reg Sci Technol* 194:103428. <https://doi.org/10.1016/j.coldregions.2021.103428>
- Peters-Lidard CD, Blackburn E, Liang X (1998) The effect of soil thermal conductivity parameterization on surface energy fluxes and temperatures. *J Atmos Sci* 55(7):1209–1224. [https://doi.org/10.1175/1520-0469\(1998\)055%3c1209:TEOSTC%3e2.0.CO;2](https://doi.org/10.1175/1520-0469(1998)055%3c1209:TEOSTC%3e2.0.CO;2)
- Qin Y, Wu T, Zhao L, Wu X, Li R, Xie C, Pang Q, Hu G, Qiao Y, Zhao G, Liu G, Zhu X, Hao J (2017) Numerical modeling of the active layer thickness and permafrost thermal state across Qinghai-Tibetan Plateau. *J Geophys Res: Atmos* 122(21):11604–11620. <https://doi.org/10.1002/2017jd026858>
- Qin Y, Zhang P, Liu W, Guo Z, Xue S (2020) The application of elevation corrected MERRA2 reanalysis ground surface temperature in a permafrost model on the Qinghai-Tibet Plateau. *Cold Reg Sci Technol* 175:103067. <https://doi.org/10.1016/j.coldregions.2020.103067>

- Ran Y, Li X, Cheng G (2018) Climate warming over the past half century has led to thermal degradation of permafrost on the Qinghai-Tibet Plateau. *Cryosphere* 12(2):595–608. <https://doi.org/10.5194/tc-12-595-2018>
- Riseborough D, Shiklomanov N, Eitzelmüller B, Gruber S, Marchenko S (2008) Recent advances in permafrost modelling. *Permafrost Periglac Process* 19:137–156
- Sargam Y, Wang K, Cho IH (2021) Machine learning based prediction model for thermal conductivity of concrete. *J Build Eng* 34:101956. <https://doi.org/10.1016/j.jobte.2020.101956>
- Shangguan W, Dai Y, Liu B, Zhu A, Duan Q, Wu L, Ji D, Ye A, Yuan H, Zhang Q, Chen D, Chen M, Chu J, Dou Y, Guo J, Li H, Li J, Liang L, Liang X, Liu H, Liu S, Miao C, Zhang Y (2013) A China data set of soil properties for land surface modeling. *J Adv Model Earth Syst* 5(2):212–224. <https://doi.org/10.1002/jame.20026>
- Shi X, Yu D, Warner E, Pan X, Petersen G, Gong Z, Weindorf D (2004) Soil database of 1:1,000,000 digital soil survey and reference system of the Chinese genetic soil classification system. *Soil Horizons* 45(4):129. <https://doi.org/10.2136/sh2004.4.0129>
- Smith WO (1942) The thermal conductivity of dry soil. *Soil Sci* 53(6):435–460
- Smith WO, Byers HG (1938) The thermal conductivity of dry soils of certain of the great soil groups I. *Soil Sci Soc Am J* 3(3C):13–19
- Tang M, Sheng Z, Chen Y (1979) On climatic characteristics of the Xizang Plateau monsoon. *Acta Geograph Sin* 34(1):34–42
- Tao Z, Zhang J (1983) The thermal conductivity of thawed and frozen soils with high water (ice) content. *J Glaciol Cryopedol* 5:75–80 ((In Chinese))
- Tarnawski V, Wagner B (1993) Modeling the thermal conductivity of frozen soil. *Cold Reg Sci Technol* 22(1):19–31. [https://doi.org/10.1016/0165-232X\(93\)90043-8](https://doi.org/10.1016/0165-232X(93)90043-8)
- Teng J, Kou J, Yan X, Zhang S, Sheng D (2020) Parameterization of soil freezing characteristic curve for unsaturated soils. *Cold Reg Sci Technol* 170:102928. <https://doi.org/10.1016/j.coldregions.2019.102928>
- Tian Z, Lu Y, Horton R, Ren T (2016) A simplified de Vries-based model to estimate thermal conductivity of unfrozen and frozen soil. *Eur J Soil Sci* 67(5):564–572. <https://doi.org/10.1111/ejss.12366>
- Tian Z, Ren T, Heitman JL, Horton R (2020) Estimating thermal conductivity of frozen soils from air-filled porosity. *Soil Sci Soc Am J* 84(5):1650–1657. <https://doi.org/10.1002/saj2.20102>
- Wang C, Yang K (2018) A new scheme for considering soil water-heat transport coupling based on Community Land Model: model description and preliminary validation. *J Adv Model Earth Syst* 10:927–950
- Wang Z, Wang Q, Zhao L, Wu X, Yue G, Zou D, Nan Z, Liu G, Pang Q, Fang H, Wu T, Shi J, Jiao K, Zhao Y, Zhang L (2016) Mapping the vegetation distribution of the permafrost zone on the Qinghai-Tibet Plateau. *J Mt Sci* 13(6):1035–1046. <https://doi.org/10.1007/s11629-015-3485-y>
- Wang X, Yang Y, Lv J, He H (2023) Past, present and future of the applications of machine learning in soil science and hydrology. *Soil Water Res* 18(2):67–80. <https://doi.org/10.17221/94/2022-swr>
- Xu X, Wu Q (2019) Impact of climate change on allowable bearing capacity on the Qinghai-Tibetan Plateau. *Adv Clim Chang Res* 2:99–108
- Yan H, He H, Dyck M, Jin H, Li M, Si B, Lv J (2019) A generalized model for estimating effective soil thermal conductivity based on the Kasubuchi algorithm. *Geoderma* 353:227–242. <https://doi.org/10.1016/j.geoderma.2019.06.031>
- Yan X, Duan Z, Sun Q (2021) Influences of water and salt contents on the thermal conductivity of loess. *Environ Earth Sci* 80:1–14. <https://doi.org/10.1007/s12665-020-09335-2>
- Yang K, Wang C (2019) Water storage effect of soil freeze-thaw process and its impacts on soil hydro-thermal regime variations. *Agric For Meteorol* 265:280–294. <https://doi.org/10.1016/j.agrfor.2018.11.011>
- Yang K, Koike T, Ye BS, Bastidas L (2005) Inverse analysis of the role of soil vertical heterogeneity in controlling surface soil state and energy partition. *J Geophys Res* 110:D08101. <https://doi.org/10.1029/2004JD005000>
- Yang Y, Fang J, Pan Y, Ji C (2009) Aboveground biomass in Tibetan grasslands. *J Arid Environ* 73(1):91–95. <https://doi.org/10.1016/j.jaridenv.2008.09.027>
- Yang S, Li R, Wu T, Hu G, Xiao Y, Du Y, Zhu X, Ni J, Ma J, Zhang Y, Shi J, Qiao Y (2020) Evaluation of reanalysis soil temperature and soil moisture products in permafrost regions on the Qinghai-Tibetan Plateau. *Geoderma*. <https://doi.org/10.1016/j.geoderma.2020.114583>
- Yang S, Li R, Wu T, Wu X, Zhao L, Hu G et al (2021) Evaluation of soil thermal conductivity schemes incorporated into CLM5.0 in permafrost regions on the Tibetan Plateau. *Geoderma* 401:115330
- Yu L, Feng C, Li X, Cui Y (2015) Recent progress in the impact of the heat sources over Tibetan Plateau on summer precipitation over southwest China. *Plateau Mt Meteorol Res* 35(04):91–95 ((in Chinese))
- Yu X, Asheesh P, Zhang N, Thapa B, Tjuatja S (2014) Thermo-TDR probe for measurement of soil moisture, density, and thermal properties. In *Geo-Congress 2014: Geo-characterization and Modeling for Sustainability*, pp 2804–2813. <https://doi.org/10.1061/9780784413272.271>
- Yue G, Zhao L, Wang Z, Zhang L, Zou D, Niu L, Zhao Y, Qiao Y (2017) Spatial variation in biomass and its relationships to soil properties in the permafrost regions along the Qinghai-Tibet Railway. *Environ Eng Sci* 34(2):130–137. <https://doi.org/10.1089/ees.2014.0504>
- Zhang M, Pei W, Li S, Lu J, Jin L (2017a) Experimental and numerical analyses of the thermo-mechanical stability of an embankment with shady and sunny slopes in a permafrost region. *Appl Therm Eng* 127:1478–1487. <https://doi.org/10.1016/j.applthermaleng.2017.08>
- Zhang W, Zhou T, Zhang L (2017b) Wetting and greening Tibetan Plateau in early summer in recent decades. *J Geophys Res Atmos* 122(11):5808–5822. <https://doi.org/10.1002/2017JD026468>
- Zhang N, Zou H, Zhang L, Puppala AJ, Liu S, Cai G (2020a) A unified soil thermal conductivity model based on artificial neural network. *Int J Therm Sci* 155:106414. <https://doi.org/10.1016/j.ijthermalsci.2020.1064>
- Zhang T, Wang C, Liu S, Zhang N, Zhang T (2020b) Assessment of soil thermal conduction using artificial neural network models. *Cold Reg Sci Technol* 169:102907. <https://doi.org/10.1016/j.coldregions.2019.102907>
- Zhao L, Ping C-L, Yang D, Cheng G, Ding Y, Liu S (2004) Changes of climate and seasonally frozen ground over the past 30 years in Qinghai-Xizang (Tibetan) Plateau, China. *Glob Planet Chang* 43(1–2):19–31. <https://doi.org/10.1016/j.gloplacha.2004.02.003>
- Zhao L, Wu T, Xie C, Li R, Wu X, Yao J, Yue G, Xiao Y (2017) Support geoscience research, environmental management, and engineering construction with investigation and monitoring on permafrost in the Qinghai-Tibet Plateau, China. *Bull Chin Acad Sci (Chinese Version)* 32(10):1159–1168. <https://doi.org/10.16418/j.issn.1000-3045.2017.10.015>

- Zhao L, Hu G, Zou D, Wu X, Ma L, Sun Z, Yuan L, Zhou H, Liu S (2019a) Permafrost changes and its effects on hydrological processes on Qinghai-Tibet Plateau. *Bull Chin Acad Sci (Chinese Version)* 34(11):1233–1246. <https://doi.org/10.16418/j.issn.1000-3045.2019.11.006>
- Zhao X, Zhou G, Jiang X (2019b) Measurement of thermal conductivity for frozen soil at temperatures close to 0°C. *Measurement* 140:504–510
- Zhao Y, Si B, Zhang Z, Li M, He H, Hill RL (2019c) A new thermal conductivity model for sandy and peat soils. *Agric For Meteorol* 274:95–105. <https://doi.org/10.1016/j.agrformet.2019.04.004>
- Zhao L, Zou D, Hu G, Wu T, Du E, Liu G, Xiao Y, Li R, Pang Q, Qiao Y (2021) A synthesis dataset of permafrost thermal state for the Qinghai-Xizang (Tibet) Plateau, China. *Earth Syst Sci Data* 13(8):4207–4218. <https://doi.org/10.5194/essd-13-4207-2021>
- Zhao Y, Si B (2019) Thermal properties of sandy and peat soils under unfrozen and frozen conditions. *Soil Tillage Res* 189:64–72. <https://doi.org/10.1016/j.still.2018.12.026>
- Zou D, Zhao L, Sheng Y, Chen J, Hu G, Wu T, Wu J, Xie C, Wu X, Pang Q, Wang W, Du E, Li W, Liu G, Li J, Qin Y, Qiao Y, Wang Z, Shi J, Cheng G (2017) A new map of the permafrost distribution on the Tibetan Plateau. *Cryosphere* 11(6):2527–2542. <https://doi.org/10.5194/tc-11-2527-2017>

Publisher's Note Springer Nature remains neutral with regard to jurisdictional claims in published maps and institutional affiliations.

Springer Nature or its licensor (e.g. a society or other partner) holds exclusive rights to this article under a publishing agreement with the author(s) or other rightsholder(s); author self-archiving of the accepted manuscript version of this article is solely governed by the terms of such publishing agreement and applicable law.